JOURNAL OF MATERIALS SCIENCE 25 (1990) 353–373

The effect of particle size distribution on the rheology of an industrial suspension

D. C-H. CHENG, A. P. KRUSZEWSKI, J. R. SENIOR
Warren Spring Laboratory, Stevenage, Herts SG1 2BX, UK

T. A. ROBERTS
ICI Dental, ICI Pharmaceuticals, Macclesfield, Cheshire, SK10 2NA, UK

The viscosity of a proprietary dental composite material, consisting of suspensions of crushed glass in a polymeric liquid of a 50/50 w/w urethane dimethacrylate and triethylene glycol dimethacrylate mixture has been measured using a tube viscometer. Narrow-sized fine (ultimate particle size of 0.2 μm, which agglomerate to form particles with a mean diameter of 0.05 μm), medium (d_{50} = 1.7 μm) and coarse (25.5 μm) particle fractions were used as well as bimodal and trimodal mixtures. Total solids concentrations from 17% to 76(77)% by volume were covered. The results were analysed using extensions of the Farris theory for mixtures and reduced to the viscosity functions, h_i (φ_i), for the three monomodal fractions. They were fitted to the Mooney, Krieger–Dougherty or the three-parameter Cheng equation. The effect of particle size distribution on the Krieger–Dougherty parameters is discussed. The viscosity functions summarize the experimental results and allow the viscosities of bimodal and trimodal mixtures not measured to be predicted. The use of the predictions for the formulation of the dental material is discussed. The methodology described can be used in the design of other suspension products.

1. Introduction

This paper describes an invesigation into the effect of particle size distribution (PSD) in the shear viscosity of a proprietary dental composite material, "Occlusin" for class I and II restorations. This is a light-cured alternative to amalgam, made up of a mixture of very ligh concentration of an inorganic filler suspended in a polymeric liquid. The filler is a mixture of three size fractions of crushed glass. The suspending liquid is composed of a resin of 50/50 w/w urethane dimethacrylate and triethylene glycol dimethacrylate mixture, camphorquinone tertiary amine catalyst and surfactants, of which there are two sets. The purpose of the work is the determination of the mix of filler particle sizes to impart optimal properties on the product in respect of manufacture, ease of use by the dentist and properties after being placed and cured.

It is known, although not generally as yet, that the measurement of the viscosity of high solid content materials, or dense suspensions, is not a straightforward problem [1–3]. This means that a rather elaborate programme of measurements has to be carried out if one is interested in understanding the fundamental properties of dense suspensions. Such a programme, because of the time and cost involved, cannot usually be contemplated in an industrial research laboratory. However, simpler measurements can be carried out and the results, even though incomplete in a scientific sense, can be useful industrially if they are interpreted appropriately. This paper will illustrate this fact.

We have obtained tube viscometer results on dense suspensions and, using existing knowledge of the rheology of suspensions, interpreted the viscosity concentration relationships and the effect of PSD. In this way, limited data have been used to make predictions on optimal particle size distributions. The methodology used can be useful in solving other rheological problems in industry.

2. Experimental

2.1. Material

The filler particles were crushed borosilicate glass of three size fractions. The actual size distributions, as measured using a Micro-Meritics Sedigraph, are shown on Fig. 1. The fines were a fumed silica (0X50) supplied by Degussa. It had a nominal ultimate particle size of 0.02 μm, which agglomerated to form particles of mean diameter 0.05 μm. The fines particle size distribution was not measured. Some PSD parameters have been extracted and given in Table I.

The polymer resin was a 50/50 w/w of urethane dimethacrylate and triethylene glycol dimethacrylate. Its viscosity over a range of temperatures is shown on Fig. 2.

TABLE I Particle size distribution parameters

	d_{25} (μm)	d_{50} (μm)	d_{75} (μm)	$\frac{d_{75}}{d_{25}}$
Coarse	23	25.5	31	1.3478
Med	1.1	1.7	2.4	2.18
Fine	–	(0.05)	–	(3 say)

0022–2461/90 $03.00 + .12

TABLE II Summary of tests carried out

Code	Composition (Vol/Total Vol						Viscometer tube		Temperature T (°C)	Shear Rate Range (sec^{-1})		$\eta_S(T)$ (Pa sec)	$\eta_{R(20)}$
	V_F part	V_F surf	V_M part	V_M surf	V_C part	V_0	Length (mm)	Diameter (mm)					
1:1	0.167	0.0176				0.8148	16	1	20	1.21×10^2	9.67×10^3	4.75×10^1	1.76×10^1
1:2	0.234	0.0244				0.7419	32	2	17	1.51×10^1	1.2×10^3	1.11×10^2	3.37×10^1
							16	1		1.2×10^2	7.25×10^3		
1:3	0.284	0.0299				0.687	16	1	16	1.2×10^2	4.83×10^3	2.1×10^2	5.95×10^1
							32	2		1.51×10^1	1.2×10^3		
1:4	0.321	0.0341				0.6446	16	1	17	1.2×10^2	9.67×10^3	3.65×10^2	1.11×10^2
							32	2		1.51×10^1	1.2×10^3		
1:5	0.368	0.0391				0.5919	32	2	16.5	1.51×10^1	1.2×10^3	7.2×10^2	2.19×10^2
									17.5	1.51×10^1	3.02×10^2		
1:6	0.379	0.0402				0.5807	16	1	17	1.2×10^2	9.67×10^3	1.025×10^3	2.76×10^2
							32	2		1.51×10^1	1.2×10^3		
1:7	0.426	0.0451				0.5281	32	4	15	1.89×10^0	1.51×10^2	4.525×10^3	1.22×10^3
1:8	0.426	0.0451				0.5281	32	2	15.5	1.51×10^1	1.2×10^3	4.525×10^3	1.22×10^3
									15	1.51×10^1	1.51×10^3		
2:1			0.378	0.0266		0.5957	16	1	20	1.2×10^2	9.67×10^3	5.7×10^1	2.11×10^1
2:2			0.441	0.0310		0.5283	16	1	20	1.2×10^2	9.67×10^3	1.05×10^3	3.96×10^2
2:3			0.477	0.0336		0.4905	32	2	20	1.51×10^1	1.2×10^3	2.7×10^3	1.0×10^3
2:4			0.491	0.0353		0.4732	32	4	19	1.89×10^0	3.78×10^1	5.25×10^3	1.82×10^3
							32	2		1.51×10^1	6.04×10^2		
3:1	0.152	0.0157	0.093	0.0041		0.7328	16	1	20	1.2×10^2	9.67×10^3	6.0×10^1	2.22×10^1
3:2	0.136	0.0135	0.207	0.0093		0.6294	16	1	20	1.2×10^2	9.67×10^3	1.08×10^2	4.0×10^2
3:3	0.108	0.0115	0.323	0.0145		0.5341	32	2	20	1.5×10^1	1.2×10^3	2.8×10^2	1.04×10^2
3:4	0.106	0.0102	0.377	0.0169		0.4803	16	1	20	1.2×10^2	9.67×10^3	7.2×10^2	2.67×10^2
							32	2		1.51×10^1	4.53×10^2		
							32	4		1.89×10^0	1.51×10^2		
3:5	0.097	0.0092	0.433	0.0194		0.4308	32	4	20	1.89×10^0	1.13×10^2	2.15×10^3	7.96×10^2
3:6	0.215	0.0224	0.081	0.0000		0.6821	16	1	19	1.2×10^2	9.67×10^3	2.05×10^2	7.12×10^1
3:7	0.201	0.028	0.143	0.0000		0.6354	16	1	19	1.2×10^2	2.41×10^3	2.7×10^2	9.38×10^1
										1.51×10^1	1.2×10^3		
3:8	0.187	0.0194	0.203	0.0000		0.5919	32	2	19	1.51×10^1	1.2×10^3	3.05×10^2	1.06×10^2
3:9	0.181	0.0190	0.262	0.0109		0.5281	32	2	20	1.51×10^1	1.2×10^3	2.9×10^2	1.07×10^2
3:10	0.176	0.0157	0.323	0.0145		0.4793	32	2	20	1.51×10^1	6.04×10^2	6.1×10^2	2.26×10^2
3:11	0.144	0.0150	0.384	0.0000		0.4571	32	2	19	1.51×10^1	1.2×10^3	1.5×10^3	5.21×10^2
3:12	0.122	0.0129	0.433	0.0196		0.3901	32	4	22	1.89×10^0	1.51×10^2	3.8×10^3	1.55×10^3
3:13	0.326	0.0335	0.059	0.0027		0.5876	32	2	20	1.51×10^1	1.2×10^3	4.0×10^2	1.48×10^2
							16	1		1.2×10^2	9.67×10^3		
							16	1		1.2×10^2	7.25×10^2		
3:14	0.303	0.0308	0.131	0.0060		0.521	32	4	20	1.89×10^0	1.51×10^2	5.2×10^2	1.93×10^2
							16	1		1.2×10^2	9.67×10^3		
3:15	0.280	0.0276	0.203	0.0092		0.4693	32	2	20	1.51×10^1	6.04×10^2	6.0×10^2	2.22×10^2
							16	1		1.2×10^2	9.67×10^3		
							32	4		1.89×10^0	1.51×10^2		

3:16	0.262	0.0246	0.271	0.0122		0.4155	32	2	20	1.51×10^{1}	1.2×10^{3}	1.08×10^{3}	4.0×10^{2}
							32	2		1.51×10^{1}	1.51×10^{2}		
3:17	0.247	0.0244	0.313	0.0142		0.384	32	4	20	1.89×10^{0}	7.56×10^{1}	2.25×10^{3}	8.33×10^{2}
							32	4		1.89×10^{0}	1.51×10^{2}		
4:1	0.115	0.0123	0.200	0.0127	0.123	0.5371	32	2	17	1.51×10^{1}	1.21×10^{3}	2.6×10^{2}	7.65×10^{1}
							16	1	16	1.2×10^{2}	1.2×10^{3}		
4:2	0.093	0.0099	0.171	0.0109	0.250	0.4652	32	2	17	1.51×10^{1}	1.2×10^{3}	1.9×10^{2}	5.78×10^{1}
4:3	0.091	0.0098	0.158	0.010	0.307	0.4246	32	2	17	1.51×10^{1}	1.18×10^{3}	3.15×10^{2}	9.57×10^{1}
4:4	0.083	0.0088	0.154	0.010	0.326	0.4175	16	1	17	1.2×10^{2}	9.67×10^{3}	2.2×10^{2}	6.69×10^{1}
4:5	0.071	0.0075	0.125	0.0077	0.454	0.3356	32	4	18	1.89×10^{0}	1.51×10^{2}	1.15×10^{3}	3.75×10^{2}
4:6	0.066	0.0070	0.114	0.0080	0.489	0.3162	32	2	17	1.51×10^{1}	6.04×10^{2}	1.75×10^{3}	5.32×10^{2}
4:7	0.106	0.0091	0.332	0.0218	0.107	0.4236	32	4	19	1.89×10^{0}	1.51×10^{2}	8.4×10^{2}	2.92×10^{2}
4:8	0.080	0.0085	0.308	0.0174	0.218	0.3679	32	4	12.5	1.89×10^{0}	1.51×10^{2}	1.3×10^{2}	2.95×10^{1}
4:9	0.072	0.0066	0.242	0.0159	0.351	0.3080	32	2	21	1.51×10^{1}	1.2×10^{3}	1.72×10^{3}	6.72×10^{2}
4:10	0.070	0.0061	0.221	0.0145	0.408	0.2807	48	3	19	4.48×10^{0}	3.58×10^{2}	2.65×10^{3}	9.2×10^{2}
4:11	0.059	0.0062	0.228	0.0128	0.422	0.2726	32	2	18	1.51×10^{1}	6.05×10^{2}	3.6×10^{3}	1.17×10^{3}
4:12	0.171	0.0162	0.243	0.0161	0.066	0.4874	32	2	20	1.51×10^{1}	1.2×10^{3}	4.7×10^{2}	1.74×10^{2}
4:13	0.154	0.147	0.219	0.0146	0.158	0.4391	16	1	20	1.2×10^{2}	9.67×10^{3}	5.8×10^{2}	2.15×10^{2}
							32	2		1.51×10^{1}	6.04×10^{2}		
4:14	0.148	0.140	0.210	0.0139	0.193	0.4209	16	1	20	1.2×10^{2}	8.46×10^{3}	6.6×10^{2}	2.44×10^{2}
							32	2		1.51×10^{1}	4.53×10^{2}		
4:15	0.126	0.0120	0.180	0.0119	0.309	0.3605	32	2	20	1.51×10^{1}	1.2×10^{3}	8.0×10^{2}	2.96×10^{2}
							16	1		1.2×10^{2}	6.04×10^{3}		
4:16	0.113	0.0107	0.161	0.0106	0.384	0.3222	16	1	20	1.2×10^{2}	4.83×10^{3}	1.62×10^{3}	6.0×10^{2}
4:17	0.096	0.0103	0.147	0.0094	0.437	0.299	32	2	20	1.51×10^{1}	1.2×10^{3}	1.25×10^{3}	4.63×10^{2}
4:18	0.086	0.0093	0.133	0.0150	0.489	0.2676	32	2	20	1.51×10^{1}	6.04×10^{2}	4.1×10^{3}	1.52×10^{3}
4:19	0.139	0.0147	0.338	0.0222	0.063	0.4227	32	2	19	1.51×10^{1}	1.2×10^{3}	1.27×10^{3}	4.41×10^{2}
4:20	0.122	0.0129	0.296	0.0195	0.175	0.3750	32	4	18	1.89×10^{0}	1.51×10^{2}	9.1×10^{2}	2.96×10^{2}
4:21	0.108	0.0115	0.263	0.0173	0.268	0.3325	32	4	17	1.89×10^{0}	1.51×10^{2}	1.55×10^{3}	4.71×10^{2}
4:22	0.099	0.0105	0.240	0.0158	0.336	0.3001	48	3	18	4.48×10^{0}	1.79×10^{2}	2.37×10^{3}	7.72×10^{2}
4:23	0.099	0.0103	0.238	0.0156	0.341	0.2970	48	3	18	4.48×10^{0}	3.58×10^{2}	3.05×10^{3}	9.93×10^{2}
4:24	0.284	0.0301	0.081	0.0056	0.083	0.517	32	2	18	1.51×10^{1}	1.21×10^{3}	4.8×10^{2}	1.56×10^{2}
4:25	0.229	0.0244	0.066	0.0046	0.259	0.4177	32	2	17	1.51×10^{1}	1.21×10^{3}	6.6×10^{2}	2.01×10^{2}
4:26	0.219	0.0233	0.063	0.0042	0.313	0.3841	32	4	17	1.89×10^{0}	1.51×10^{2}	1.15×10^{3}	3.5×10^{2}
4:27	0.177	0.0187	0.051	0.0033	0.445	0.3101	32	4	17	1.89×10^{0}	7.56×10^{1}	1.7×10^{3}	5.17×10^{2}
4:28	0.241	0.0255	0.220	0.0147	0.075	0.4228	48	3	20	4.48×10^{0}	3.58×10^{2}	1.15×10^{3}	4.26×10^{2}
4:29	0.216	0.0228	0.197	0.0141	0.171	0.3792	48	3	20	4.48×10^{0}	3.58×10^{2}	1.28×10^{3}	4.74×10^{2}
4:30	0.189	0.0202	0.173	0.0113	0.282	0.3245	32	4	14.5	1.89×10^{0}	7.56×10^{1}	2.0×10^{3}	5.13×10^{2}
4:31	0.158	0.0167	0.144	0.0103	0.394	0.2768	32	2	17	1.51×10^{1}	1.21×10^{3}	2.2×10^{3}	6.69×10^{2}
4:32	0.143	0.0153	0.131	0.0092	0.457	0.244	32	2	17	1.51×10^{1}	2.26×10^{2}	6.0×10^{3}	1.82×10^{3}

$V_{i\text{part}}$ is the volume fraction of particles as such

$V_{i\text{surf}}$ is the volume fraction of surfactant associated with component i (V/V)

The subscripts O, C, F, M refer to suspending liquid, coarse particles, fine particles and medium particles, respectively.

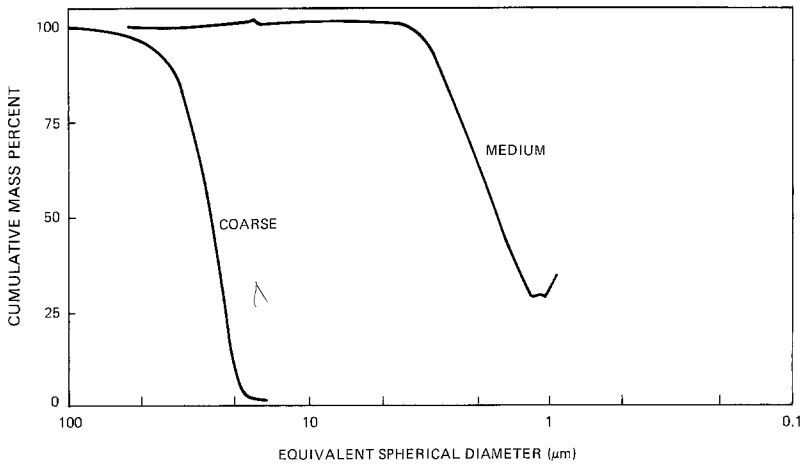

Figure 1 Particle size distributions of the filler particles

Two proprietary surfactants were used. The amounts used in each suspension were calculated based on the surface of the filler, so that a layer would be adsorbed onto the surface of the particles assumed to be spherical. The actual amounts used are given in Table II. The large particles were not coated with a surface.

A pre-mix was prepared by adding the fine particle size filler to the resin in a dough mixer. After mixing the material was transferred to a twin roll mill for further processing. This produced the final suspension of the filler in resin. The medium size filler (2 μm) was similarly mixed with resin and additives in a dough mixer and twin roll mill. The two separate suspensions of fine and medium size fillers in resin were then placed in a dough mixer and the large fraction (25 μm) filler was added during mixing. The material was then processed further on a twin roll mill. No catalyst was added to suspensions made for rheological testing.

2.2. Viscometer used

The viscometer used was a standard Davenport Piston Extrusion Rheometer (supplied by Daventest Ltd, Welwyn Garden City, Hertfordshire). This has been developed from the original design of Benbow *et al.* [4]. A description of an earlier commercial version is given in Cheng [5].

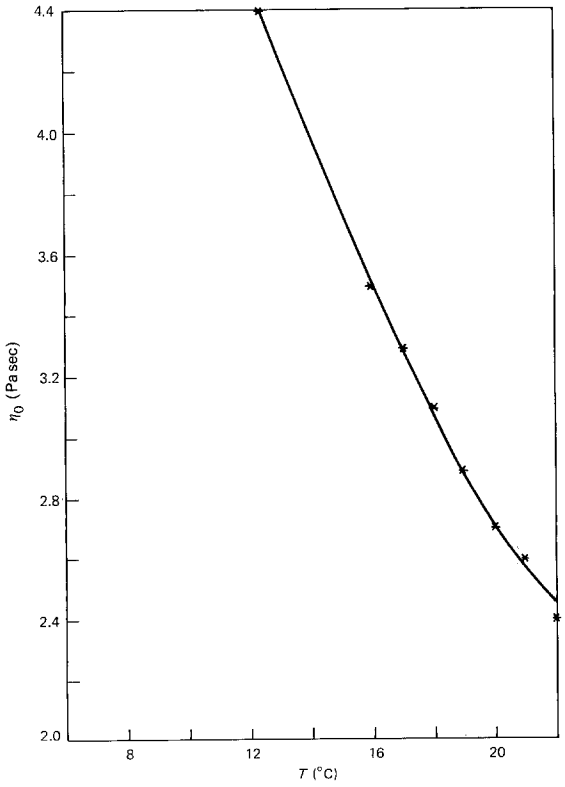

Figure 2 Viscosity of suspending liquid plotted against temperature.

2.3. Experimental procedure

The material was placed in a barrel which had an extrusion die at the exit end. Different size dies were used. The material was extruded through the die by a piston the speed of which can be varied. As material was forced through the die the pressure was measured by a pressure transducer. From the piston speed and corresponding pressure, shear rate and shear stress values were calculated. Measurements at a series of piston speeds gave a number of values of shear rate and shear stress.

The orifice die pressure P_0, in (Pa) was measured to take into account the end effect [6]. The orifice die was a shallow convergent cone varying in thickness from 1 to 3 mm depending on the diameter of the outlet. (The smaller the die outlet diameter the thicker the orifice die.)

A summary of the tests carried out is set out in Table II.

2.4. Preliminary data treatment

2.4.1. End-effect correction, and shear stress and shear rate calculation

The initial data reduction was carried out according to Cogswell [6]. End-effect correction was made by subtracting the orifice die pressure, P_0, from the tube pressure, P_L. The shear stress was then calculated using the equation

$$\tau_w = \frac{D}{4}\frac{P_L - P_0}{L} \quad (1)$$

where τ_w is the wall shear stress (Pa), D the tube diameter (m) and L the tube length (m). The apparent shear rate was calculated from the volume flowrate, Q, ($m^3 sec^{-1}$)

$$\dot{\gamma}_A = \frac{320}{\pi D^3} \quad (2)$$

where $\dot{\gamma}_A$ is the apparent shear rate (sec^{-1}).The plots of τ_w against $\dot{\gamma}_A$ are given in Figs. 3 to 13.

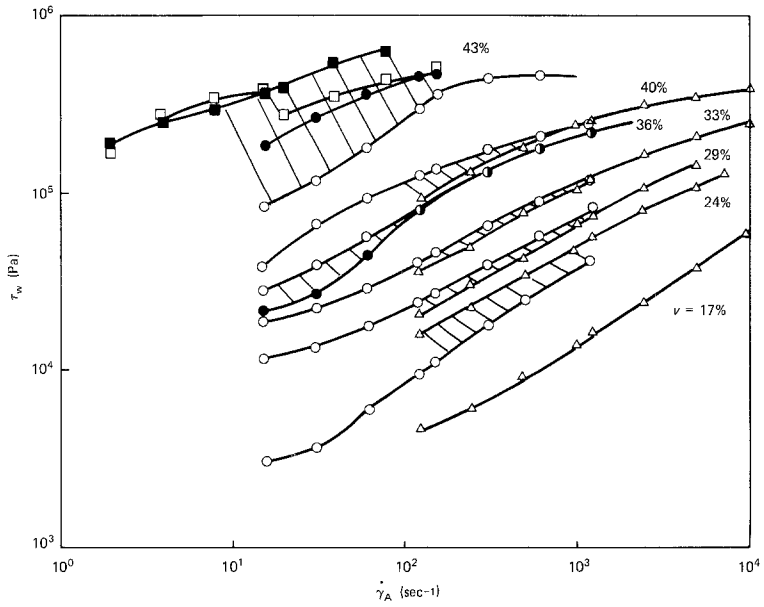

Figure 3 Flow curves for monomodal fines suspensions (tube dimensions: (△▲ 16 × 1 mm, ○● 32 × 2 mm, □■ 32 × 4 mm)

2.4.2. Preliminary assessment of flow curve results

The flow curves on Figs 3 to 13 are clearly non-Newtonian and do not follow any of the well known models, such as power law, Bingham plastic, Casson and Cross. If one general shape is to be ascribed to the suspensions as a whole, the master flow curve would show a yield stress as the shear rate tends to zero. As the shear rate increases, it curves upwards, but only to level out again to give an upper constant stress as shear rate becomes very large. The inflexion shear rate decreases as the concentration increases.

For the very high concentrations, there is a suggestion that the curve does not level out entirely, but that it curves upwards again as the shear rate is increased. In two distinct cases, Figs 3 and 10, the flow curve shows a discontinuity which is reminiscent of behaviour in rotation viscometers [1]. This must be germane to the fact that flow curves of very high concentration suspensions do not always follow the master curve as described above.

The results for the monomodal fines suspensions (Fig. 3) show, as expected, an increase in viscosity as concentration is increased. However, results obtained using tubes of different diameters do not agree. Even with identical tubes, there are large differences. Both effects appear to increase as concentration is increased. Monomodal medium suspensions also show the diameter effect (Fig. 4).

The bimodal suspensions based on 17% fines appear to be well-behaved (Fig. 5). Those based on higher fines concentrations gave viscosities which decreased as medium particles were added over a certain concentration range (Figs 6 and 7). The data at 15.1 and 120 s^{-1} were replotted against concentration to bring out this behaviour (Figs. 14 and 15). They also emphasize that the bimodal results were subject to both poor reproducibility and the diameter effect, particularly in Figs 7 and 15.

Most of the trimodal data do not show viscosity reduction with increase of concentration, except on Figs 8 and 11. Again the data have been replotted in Figs 16 and 17. The viscosity in Fig. 16 appears to oscillate with concentration, which does not seem likely to be due to poor reproducibility. The data for the trimodal suspensions are not as comprehensive as

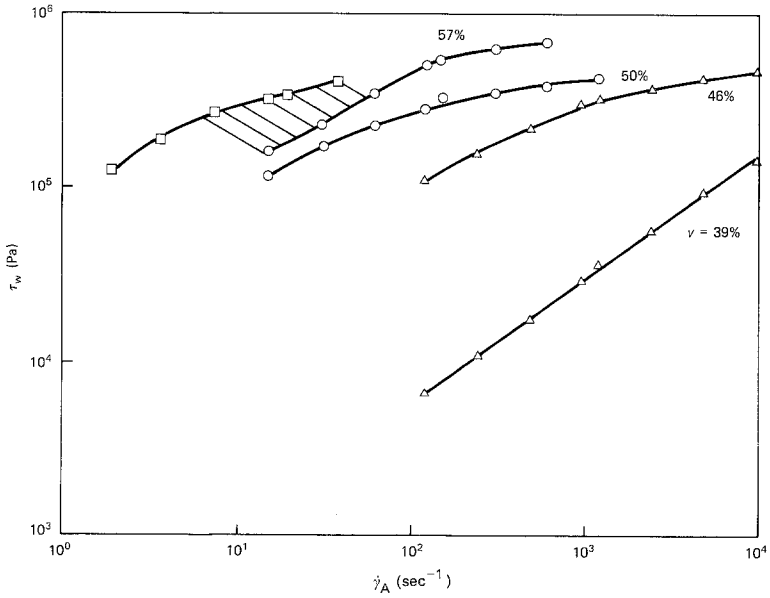

Figure 4 Flow curves for monomodal mediums suspensions (tube dimensions: △ 16 × 1 mm, ○ 32 × 2 mm, □ 32 × 4 mm).

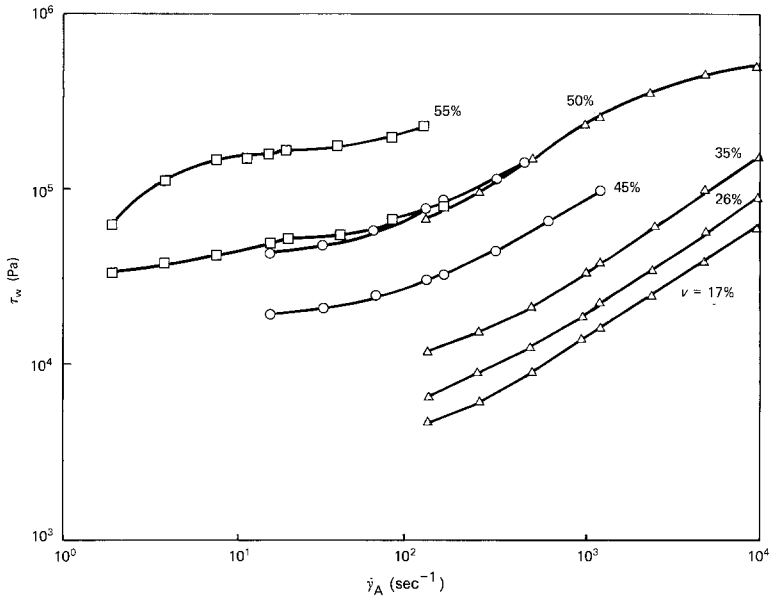

Figure 5 Flow curves for bimodal (17% fines + mediums) suspensions (tube dimensions: △ 16 × 1 mm, ○ 32 × 2 mm, □ 32 × 4 mm).

the bimodals, but what is available (Figs 9 and 10) suggests that their scatter and diameter effect were not as bad.

2.4.3. Interpolation for viscosity at 100 sec^{-1}

The dependence of the suspension viscosity on shear rate and PSD is clearly a complex matter. It does not seem possible to use the flow curves as they stand to make predictions. It was decided to concentrate on a specific shear rate of 100 sec^{-1} to make further progress. The plotted flow curves were interpolated (and extrapolated in some cases) by eye to obtain the 100 sec^{-1} viscosity. These values are given in Table II.

2.4.4. Temperature correction

Test temperatures varied widely between 12.5 and 22° C (Table II). It was therefore necessary to correct for temperature. This was done by assuming that the viscosity–temperature relationship of the suspension was given by that of the suspending liquid alone, i.e.

$$\eta_s\,(20) = \frac{\eta_0\,(20)}{\eta_0\,(T)}\,\eta_s\,(T) \qquad (3)$$

where $\eta_s\,(T)$ is the suspension viscosity at 100 sec^{-1} at temperature T, irrespective of monomodal or mixed suspension and $\eta_0\,(T)$ is the viscosity of the suspending liquid (Pa sec). Experimental viscosity results for the suspending liquid plotted on Fig. 2 were used. Values read off the fitted straight line were used to calculate $\eta_s\,(20)$ and η_R. The experimental $\eta_s\,(T)$ and the derived η_R are given in Table II.

2.4.5. Assessment of reproducibility

The standard viscosities, at 100 sec^{-1} and 20° C, obtained on suspensions of the same concentration and tested in tubes of the same diameter were used to assess reproducibility. They were expressed as the fractional difference and plotted on Fig. 18

$$\text{FD} = 1 - \frac{\text{smaller } \eta_s\,(20)}{\text{larger } \eta_s\,(20)} \qquad (4)$$

where FD is the fractional difference in viscosity readings for the same concentration and tube diameter.

Differences of up to 40% in FD were apparent. Of more interest, however, is the indication that (i) FD increased as concentration was increased and (ii) FD

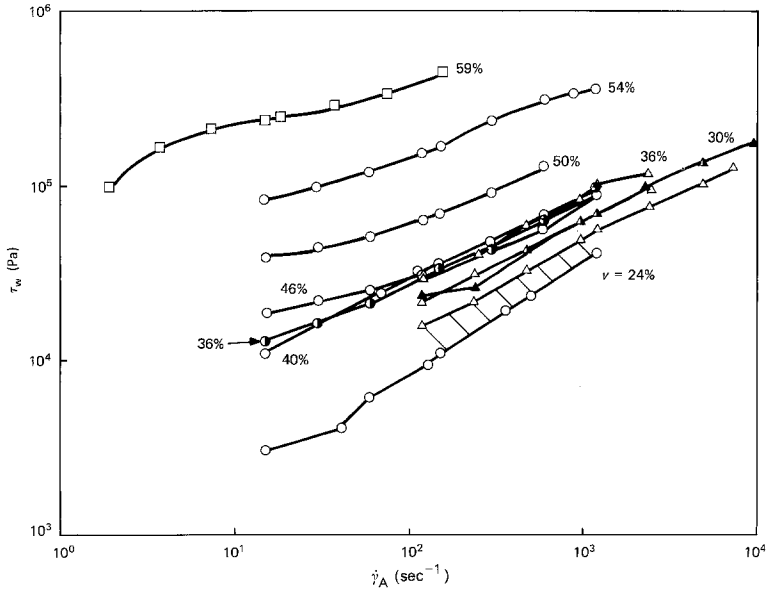

Figure 6 Flow curves for bimodal (24% fines + mediums) suspensions (tube dimensions: △▲ 16 × 1 mm, ○● 32 × 2 mm, □■ 32 × 4 mm).

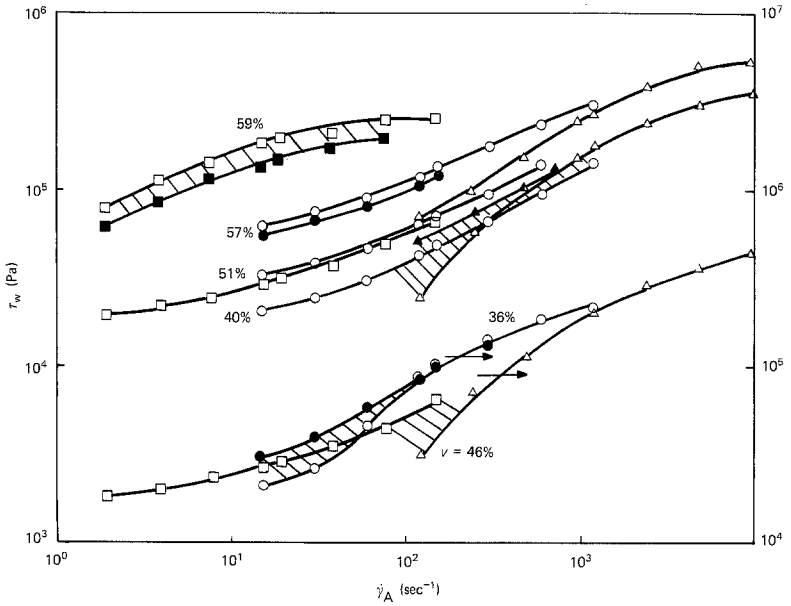

Figure 7 Flow curves for bimodal (36% fines + mediums) suspenions (tube dimenions: △▲ 16 × 1 mm, ○● 32 × 2 mm, □■ 32 × 4 mm).

was larger for the monomodal fine suspensions compared with the bimodal fine + medium suspensions. That is FD was larger for suspensions with a narrower PSD. These variations are as expected from published results on other dense suspensions [2, 3, 5].

2.4.6. Assessment of tube diameter effect

It is often found in suspensions that the τ_w against $\dot{\gamma}_A$ curves for different diameters do not fall on a master curve. If a larger tube curve lies above that of a smaller tube (i.e. has larger τ_w), the difference may be explained in terms of the wall-slip effect. The τ_w against $\dot{\gamma}_A$ curves of this work did not show such consistent behaviour. A more thorough assessment was therefore carried out in terms of the fractional difference using the 100 sec^{-1} viscosities.

$$\text{FD2} = 1 - \frac{\text{smaller tube } \eta_s\ (20)}{\text{larger tube } \eta_s\ (20)} \qquad (5)$$

where FD2 is the difference in viscosity readings for the same concentration and different tube diameter. These quantities are plotted on Fig. 19.

It can be seen that (i) values of FD2 up to 60% were obtained. This was larger than the reproducibility figure of 40% and meant that the differences between tubes of different diameters were not only caused by experimental scatter. (ii) FD2 was not always positive, which meant that the wall-slip effect cannot be the only explanation of the differences. There is a hint that (iii) FD2 was negative for low concentrations and increased to become positive at high concentrations and (iv) at the same concentration, FD2 was reduced as one goes from monomodal to bimodal and trimodal suspensions (i.e. FD2 depended on PSD).

The significance of these observations is discussed later in Section 4.1.4. Here it can be concluded that the viscosity of suspensions does depend on tube diameter. As no clear systematic variation was obtained, the differences found in the present results cannot be reduced further. They have therefore been treated as experimental scatter in the data anylsis below.

2.4.7. Calculation of effective volume concentration

The volume of surfactant in the suspension was taken into account in the calculation of the effective volume

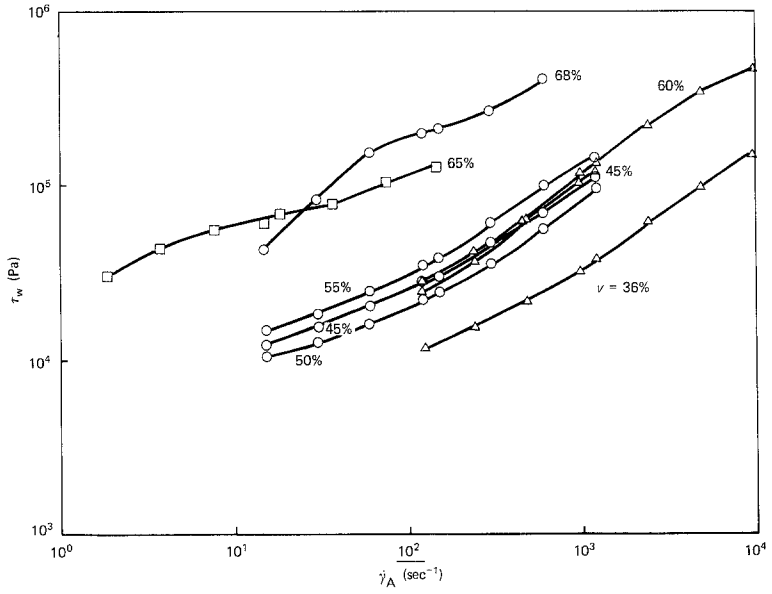

Figure 8 Flow curves for trimodal [(17% fines + mediums) 36% + coarse] suspensions (tube dimensions: △ 16 × 1 mm, ○ 32 × 2 mm, □ 32 × 4 mm).

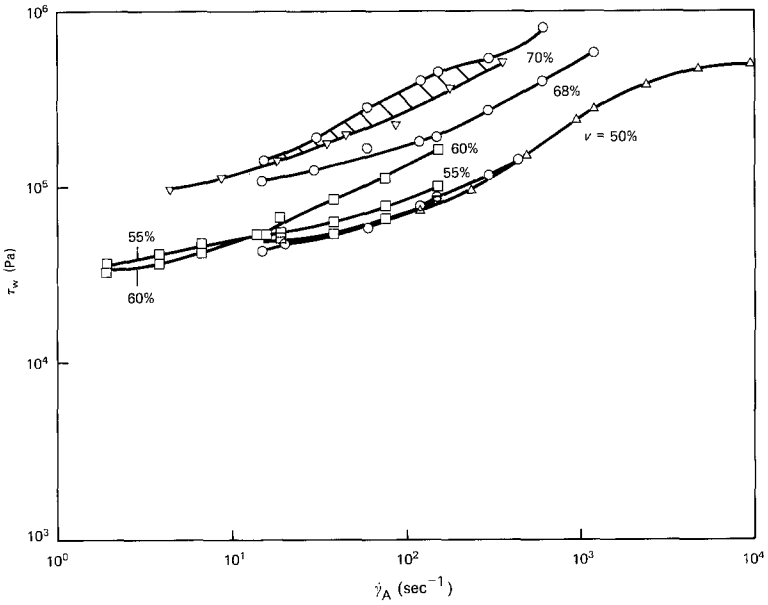

Figure 9 Flow curves for trimodal [(17% fines + mediums) 50% + coarse] suspensions (tube dimensions: △ 16 × 1 mm², ○ 32 × 2 mm², ▽ 48 × 3 mm², □ 32 × 4 mm²)

concentrations. The volumes associated with the fine and medium particles are given in Table II. The volume associated with the coarse particles was assumed to be negligible. In the equations for φ in Section 3.1, the following were used

$$v_C = v_{C\text{part}} \quad v_M = v_{M\text{part}} + v_{M\text{surf}}$$
$$v_F = v_{F\text{part}} + v_{F\text{surf}} \tag{6}$$

where $V_{i\text{part}}$ is the volume fraction of particles as such and $V_{i\text{surf}}$ is the volume fraction of surfactant associated with component i (V/V). The subscripts C, M and F refer to coarse, medium and fine particles, respectively.

3. Data analysis

3.1. Theory

The relative viscosity at 100 sec^{-1}, η_R, was used in data analysis from this point on. The basis was the Farris theory [7], but his approach has been generalized as below.

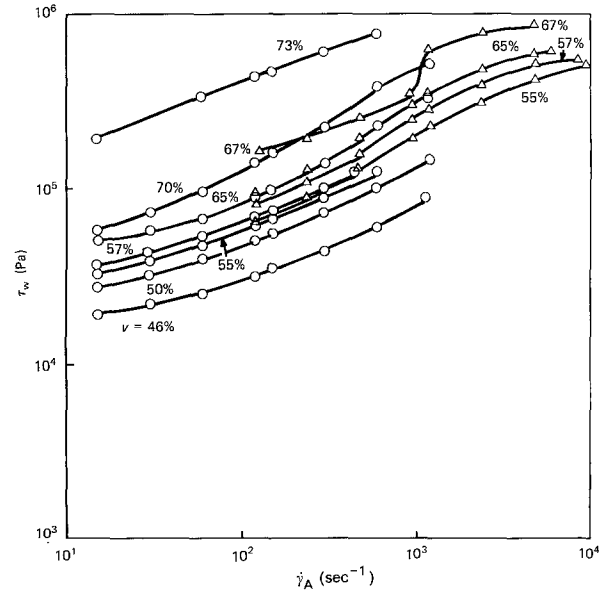

Figure 10 Flow curves for trimodal [(24% fines + mediums) 45% + coarse] suspensions (tube dimensions: △ 16 × 1 mm², ○ 32 × 2 mm²)

In Farris' theory, the viscosity of a bimodal suspension of spheres is calculated by treating the mixture of fine particles and the suspending liquid as a homogeneous fluid. If this is made up of V_0 the volume of suspending liquid and V_1 the volume of the fines, then it would have a viscosity of

$$\eta_1 = h(\varphi_1)\eta_0 \tag{7}$$

where the effective volume concentration of the fines is

$$\varphi_1 = \frac{V_1}{V_0 + V_1} \tag{8}$$

and $h(\varphi_1)$ is some function which can be determined either by theoretical modelling or experiments. If the volume of the coarse particles in the suspension is V_2 and they are considered to be suspended in the homogeneous mixture of liquid + fines, the suspension will have a viscosity of

$$\eta_s^{(2)} = h(\varphi_2)\eta_1 = h(\varphi_2)h(\varphi_1)\eta_0 \tag{9}$$

where the effective volume concentration of the coarse is

$$\varphi_2 = \frac{V_2}{V_0 + V_1 + V_2} \tag{10}$$

Thus the relative viscosity of the bimodal suspension is

$$\eta_R^{(2)} = h(\varphi_1)h(\varphi_2) \tag{11}$$

and can be calculated from the effective concentrations, φ_1 and φ_2, and the function $h(\varphi)$.

The true volume concentrations of the fines and coarse in the suspension are

$$v_1 = \frac{V_1}{V_0 + V_1 + V_2} \qquad v_2 = \frac{V_2}{V_0 + V_1 + V_2} \tag{12}$$

and the total solids concentration is

$$v = v_1 + v_2 \tag{13}$$

where V_i is the volume of component i(V/V). The effective volume concentrations can also be calculated

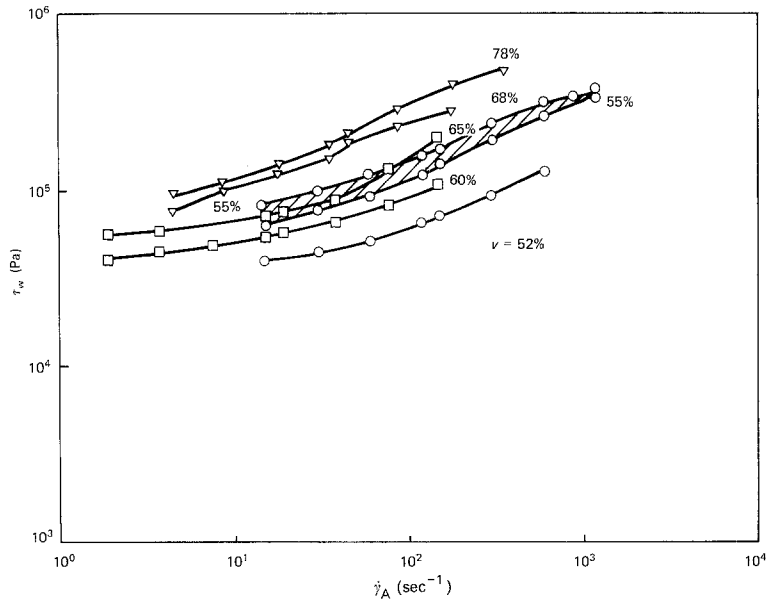

Figure 11 Flow curves for trimodal [(24% fines + mediums) 52% + coarse] suspensions (tube dimensions: ○ 32 × 2 mm^2, ▽ 48 × 3 mm^2, □ 32 × 4 mm^2)

from these equations

$$\varphi_1 = \frac{v_1}{1 - v_2} \qquad \varphi_2 = v_2 \tag{14}$$

Also

$$(1 - v) = (1 - \varphi_1)(1 - \varphi_2) \tag{15}$$

The relative viscosity of a trimodal suspension can be derived in the same way, by assuming that the mixture of suspending liquid + fines + mediums behaves as a homogeneous fluid to the coarse, and the mixture of liquid + fines behaves as homogeneous to the mediums. It is

$$\eta_R^{(3)} = h(\varphi_1)h(\varphi_2)h(\varphi_3) \tag{16}$$

Where

$$\varphi_1 = \frac{v_1}{1 - v_2 - v_3} \qquad \varphi_2 = \frac{v_2}{1 - v_3} \qquad \varphi_3 = v_3 \tag{17}$$

$$(1 - v) = (1 - \varphi_1)(1 - \varphi_2)(1 - \varphi_3) \tag{18}$$

Farris' theory was based on various explicit and implicit assumptions which can be relaxed to make it more generally applicable. The first assumption is that the particles are spherical, but this fact is not specifically invoked in the mathematical derivation and so it seems that the approach can be applied to non-spherical particles.

Farris implicitly assumed that the particles are rigid. This will apply to suspensions of particles with adsorbed surfactant assuming that the adsorbed layer is not deformable, a reasonable assumption if the particle surfaces are fully covered by surfactants, as in this work. Section 2.4.7. describes how the volume of adsorbed surfactant is taken into account in calculating the effective volume concentrations, φ_i.

Although Farris considered mixed suspensions of fractions of particles of unique sizes, this need not be a restriction. The important criterion is that the smaller particles should be very much smaller than the larger ones, such that the mixture of liquid and the smaller particles behaves as homogeneous to the larger particles. In mixtures of narrowly sized fractions, this condition can clearly be attained when the largest particle of the smaller fraction is very much smaller than the smallest of the larger fraction. In Farris' paper, experimental results indicated that the small

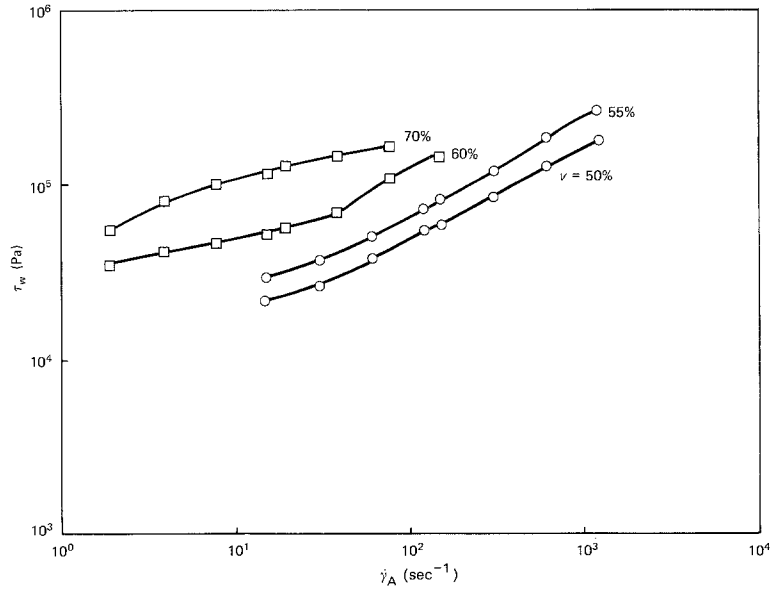

Figure 12 Flow curves for trimodal [(36% fines + mediums) 42% + coarse] suspensions (tube dimensions: ○ 32 × 2 mm^2, □ 32 × 4 mm^2)

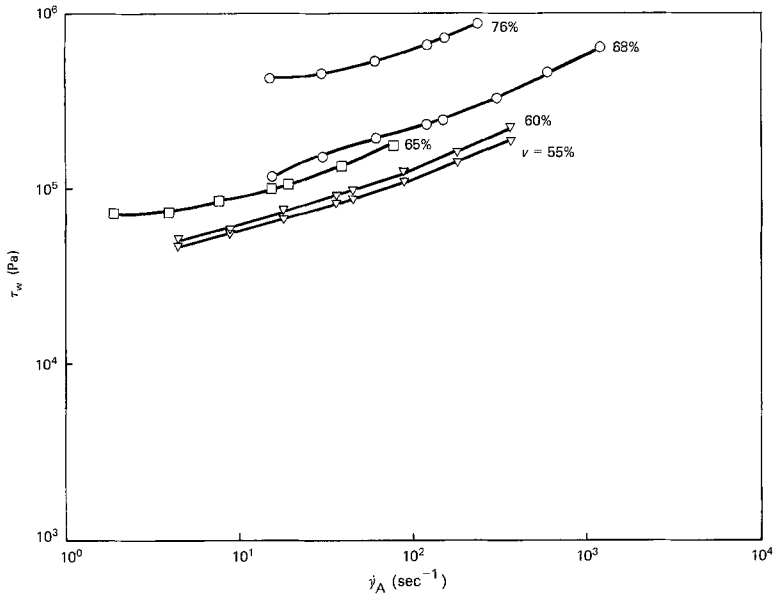

Figure 13 Flow curves for trimodal [(36% fines + mediums) 52% + coarse] suspensions (tube dimensions: ○ 32 × 2 mm, ▽ 48 × 3 mm, □ 32 × 4 mm).

particles should be less than 1/10th the size of large particles for their size to be negligible. Other theories [8, 9] do not specifically make this demand.

Farris assumed that the function $h(\varphi)$ is the same for all size fractions. This restriction is not necessary; there is experimental evidence that $h(\varphi)$ can vary with particle size and PSD. Thus Equation 7 for monomodal suspensions becomes

$$(\eta_R)_i = h_i(\varphi_i) \quad (19)$$

where $h_i(\varphi_i)$ is the viscosity function for component i the same as $(\eta_R^{(1)})$ for component i. For bimodal suspensions, Equation 11 becomes

$$\eta_R^{(2)} = h_1(\varphi_1)h_2(\varphi_2) \quad (20)$$

and for trimodal suspensions, Equations 16 becomes

$$\eta_R^{(3)} = h_1(\varphi_1)h_2(\varphi_2)h_3(\varphi_3) \quad (21)$$

In this work, we wish to explore how these generalizations of Farris' theory apply to our suspensions.

3.2. Data analysis procedure

Fig. 20 summarizes the data analysis procedure. Firstly, the experimental monomodal fines viscosity

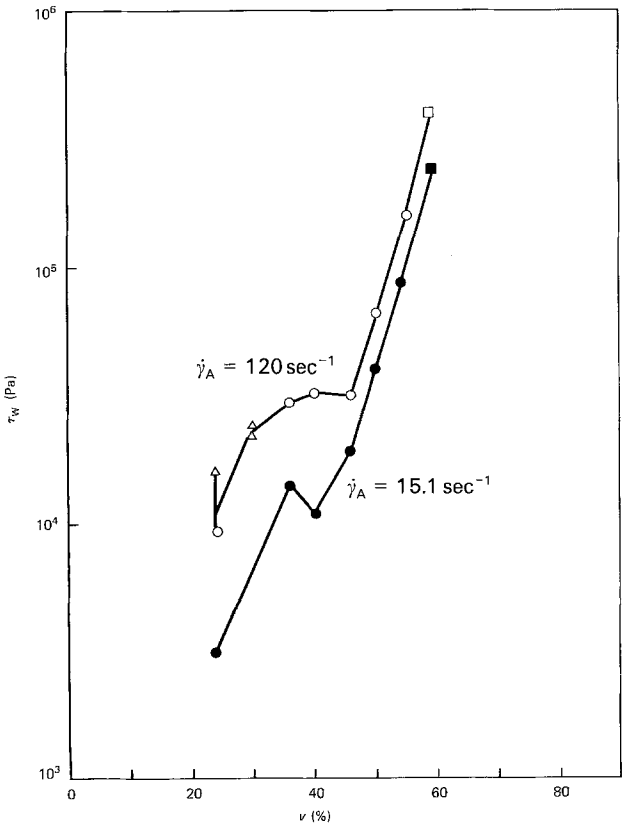

Figure 14 Variation of τ_w at given $\dot{\gamma}_A$ with concentration for bimodal (24% fines + mediums) suspensions (tube dimensions: △ 16 × 1 mm, ○● 32 × 2 mm, □■ 32 × 4 mm, ○ △ $\dot{\gamma}_A$ = 120 sec^{-1}, ● $\dot{\gamma}_A$ = 15.1 sec^{-1}).

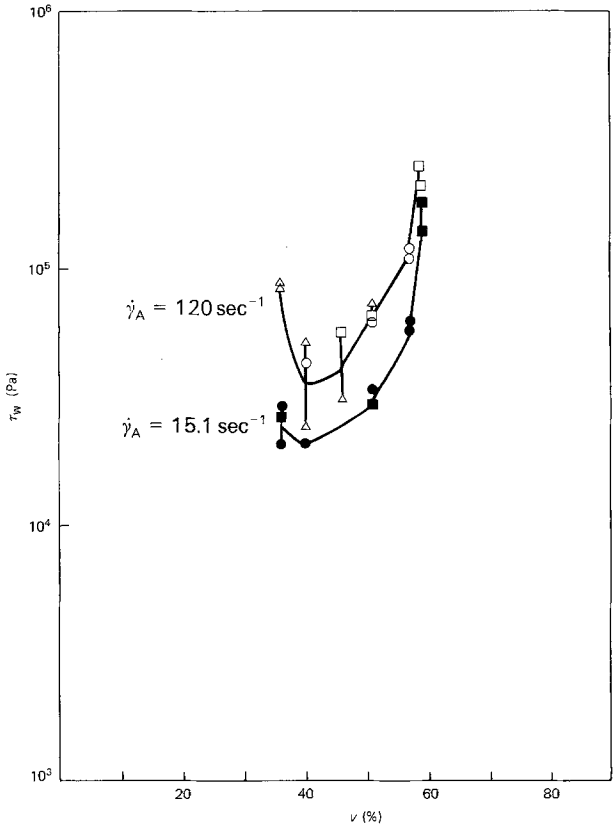

Figure 15 Variation of τ_w at given $\dot{\gamma}_A$ with concentration for bimodal (36% fines + mediums) suspensions (tube dimensions: △ 16 × 1 mm, ○● 32 × 2 mm, □■ 32 × 4 mm, △□○$\dot{\gamma}_A$ = 120 sec^{-1}, ●■$\dot{\gamma}_A$ = 15.1 sec^{-1}).

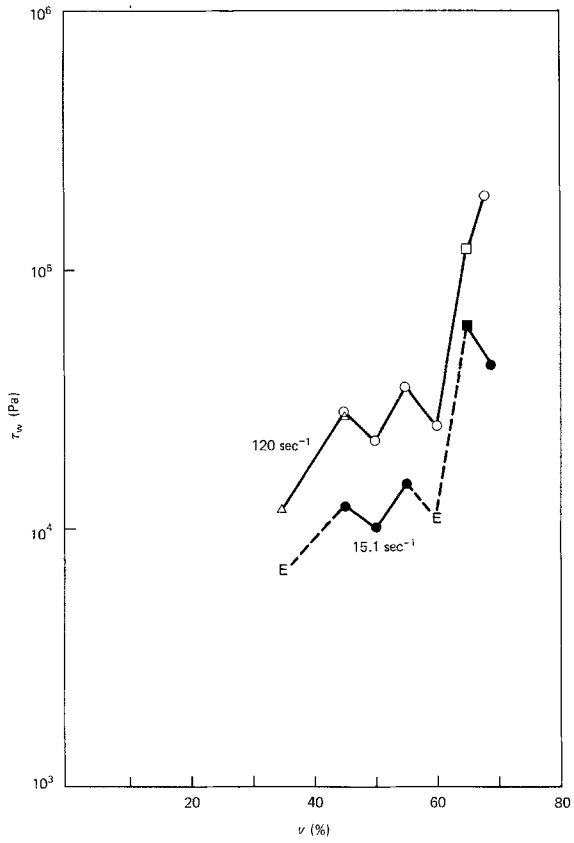

Figure 16 Variation of τ_w at given $\bar{\sigma}_A$ with concentration for trimodal [(17% fines + mediums) 36% + coarse] suspensions (tube dimensions: ○● 32 × 2 mm, □■ 32 × 4 mm, E extrapolated).

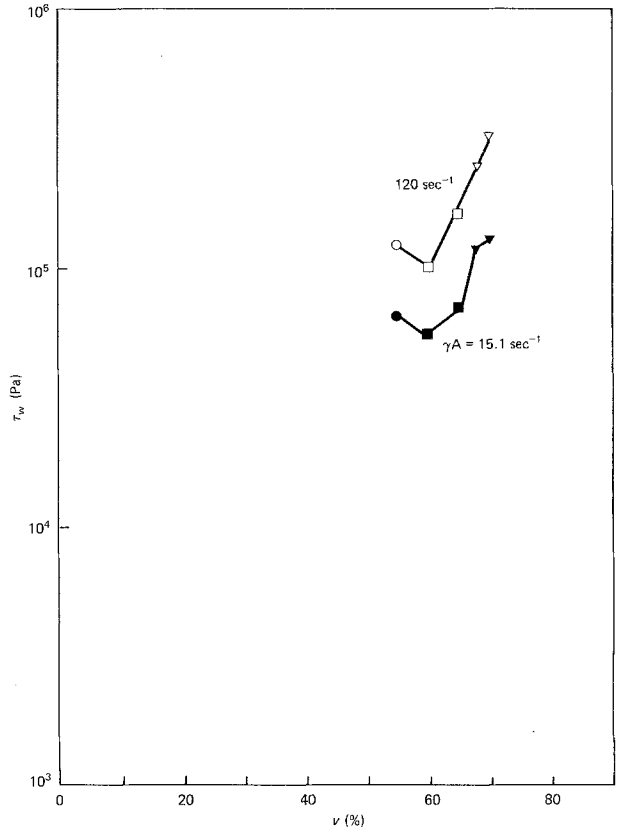

Figure 17 Variation of τ_w at given $\dot{\gamma}_A$ with concentration for trimodal [(24% fines + mediums) 52% + coarse] suspensions (tube dimensions: ○● 32 × 2 mm, ▽▼ 48 × 3 mm, □■ 32 × 4 mm).

was curve fitted to determine an equation for $h_1(\varphi_1)$, using the procedure to be described in Section 3.3.

The resulting $h_1(\varphi_1)$ equation was used with the experimental bimodal viscosity to derive $h_2(\varphi_2)$ data. From Equation 20,

$$h_2(\varphi_2) = \frac{\eta_R^{(2)}}{h_1(\varphi_1)} \tag{22}$$

These were taken together with experimental monomodal viscosity for the mediums, $(\eta_R^{(1)})_2$ and curve fitted to determine an equation $h_2(\varphi_2)$.

The resulting $h_2(\varphi_2)$ and $h_1(\varphi_1)$ equations were then used together with the experimental trimodal viscosity to derive $h_3(\varphi_3)$ data. From Equation 21,

$$h_3(\varphi_3) = \frac{\eta_R^{(3)}}{h_1(\varphi_1)h_2(\varphi_2)} \tag{23}$$

These were then curve-fitted to determine an equation for $h_3(\varphi_3)$.

The three equations for h_1, h_2 and h_3 can be used to predict the viscosity of bimodal and trimodal suspensions of any composition (Section 3.6).

3.3. Curve fitting to determine equation for $h_i(\varphi_i)$

These were then curve fitted to determine an equation suspension viscosity [10]. Amongst the more popular ones are the one-parameter Mooney equation [11]

$$\eta_R^{(1)} = \exp\left(\frac{2.5\varphi}{1 - \varphi/v_m}\right) \tag{24}$$

where v_m is the maximum volume fraction, and the two-parameter Krieger–Dougherty equation [12],

$$\eta_R^{(1)} = \left(\frac{1}{1 - \varphi/v_m}\right)^{kv_m} \tag{25}$$

These were chosen for trials in this work. Also used

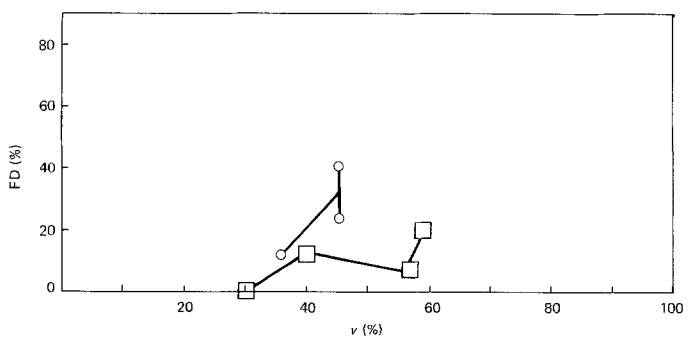

Figure 18 Reproducibility in results obtained using tube of same dimensions (○ monomodal fines, □ bimodal (fines + mediums) FD = 1 - (smaller η (20)/larger η (20)).

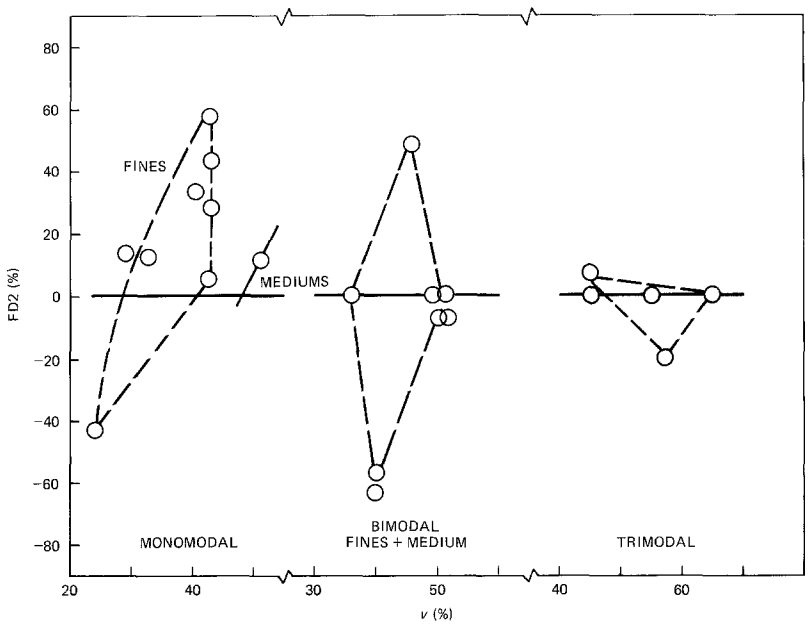

Figure 19 Effect of tube diameter (32 × 2 mm and 32 × 4 mm tubes) FD2 = 1 - (smaller tube η (20)/bigger tube η (20)).

was the equation proposed by Cheng [10]

$$\eta_R^{(1)} = \frac{1 + A\varphi + B\varphi^2}{1 - (\varphi/V_m)^{1/3}} \quad (26)$$

where A and B are constants.

The general form of the Cheng equation allows for polynomials of increasing order to be used as the numerator if the data so warrant. In this work the three-parameter version was used. All three equations have the two necessary features, (i) $\eta_R^{(1)} = 1$ at $\varphi = 0$ and (ii) $\eta_R^{(1)}$ tending to infinity as φ tends to v_m.

In the curve fitting, we wished to determine which of the three equations best fit the data and also to determine the best values of the parameters for the fitted equation. The criterion for best fit was chosen to be minimum averaged residue

$$R = \frac{[\Sigma|\log\log(\text{expt } \eta_R^{(1)}) - \log\log(\text{cal } \eta_R^{(1)})|]}{\text{number of data points}} \quad (27)$$

The reason for using log log $\eta_R^{(1)}$ is this. Experimental data of viscosity against concentration are known to become more scattered the higher the concentration [13], even when log $\eta_R^{(1)}$ is plotted against v, for example Fig. 21 [14]. However, if log log $\eta_R^{(1)}$ is plotted against v, as in Fig. 22, the data are more evenly spread about the mean curve. It can then be assumed that the spread has the same weight irrespective of concentration and the best-fit curve is obtained when

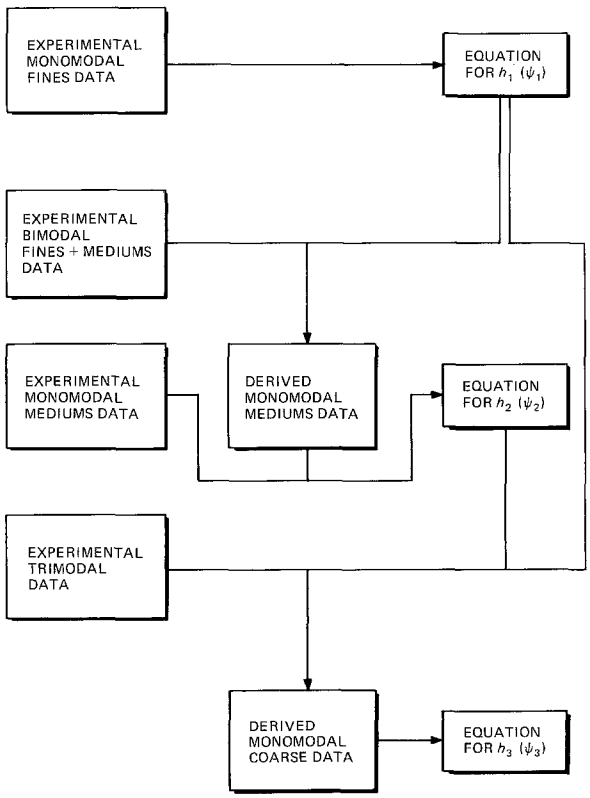

Figure 20 Data analysis procedure

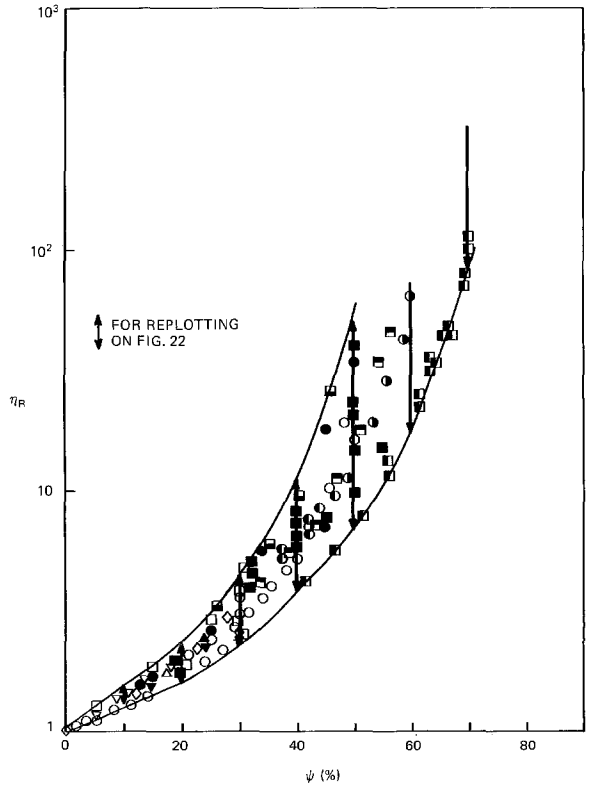

Figure 21 Literature results of suspensions viscosity plotted in the form log η_R against ψ. Taken from Thomas [13].

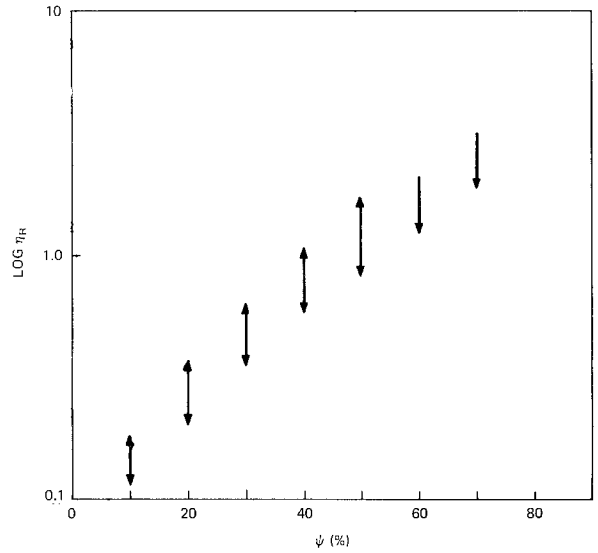

Figure 22 Data from Fig. 21 replotted in the form of log log η_R against ψ.

the average residue (or residue for short), R, is minimized as the values of the parameters are varied.

Then by comparing the minimum R for the three equations, the one with the lowest minimum R can be taken as the best-fit equation.

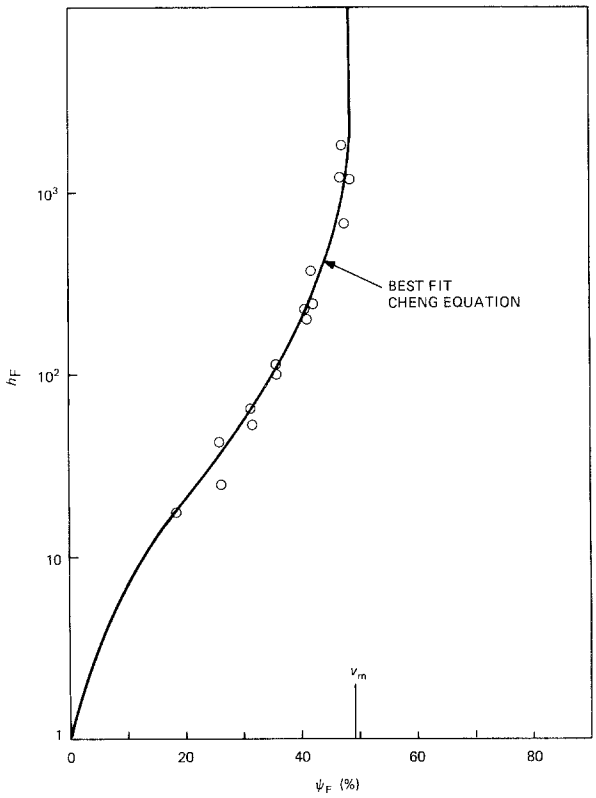

Figure 23 Viscosity function of fines suspensions. (O experimental).

3.4. Optimization procedures

With one parameter, v_m, the optimization of the Mooney equation was straightforward. The residue, R, was calculated for various values of v_m up to a maximum of 1 (as the fractional volume of particles cannot exceed unity). A plot of R against v_m then allowed the minimum R and the corresponding v_m to be determined. The accuracy chosen was three decimal places in v_m. (Note that there is also a lower limit to v_m, namely the largest v in the data being fitted.)

For the Krieger–Dougherty equation, a similar procedure was followed, with both v_m and k being varied, k is the intrinsic viscosity in the Krieger–Dougherty equation. Values of R were plotted on a two dimensional (v_m, k) graph. With sufficient values of R, the averaged residue, contour lines of constant R were drawn and the location of the minimum R and the corresponding v_m and k were found. By repeating the calculation in the minimum area, the optimal parameters were determined to the chosen accuracy of three decimal places for v_m and one decimal place for k.

For the Cheng equation, with three parameters, the optimization if made in a similar way as described above would be tedious and so a computerized search technique was used. The first method tried was the rotating simplex method [15], but this gave problems with convergence. Too large a simplex overshot the minimum. A small simplex converged in some local minimum which was far removed from the correct solution or it took a long time to find the optimum. For an efficient optimization, it is necessary to have a strategy for varying the size of the simplex as the search progresses. Because of this and other convergence problems, an alternative optimization procedure was used.

This was a slope-marching routine [16] which varies one parameter at a time, finding the direction in which R was reduced and varying the parameter until it started to increase. The next parameter was then varied similarly, and so on. In this work, the parameters were varied in the order v_m, A and B, with the conditions that v_m must not exceed 1 and A and B must be positive. The art of using this routine is to make the correct choice of step size. The Cheng equation is more sensitive to variations in v_m than A and B, and so the step size for v_m was set at 100th of the steps of A and B. Experience showed that initial steps for A and B equalling 1 gave satisfactory results. Subsequently the steps were reduced by a factor of 10, giving an accuracy of one decimal place in the final values of A and B (and 3 decimal places in the value of v_m). Although this procedure was not very fast, in that it had to calculate R at every step, it was found to be adequate for this work. (More rapid slope-marching routines are available [16] if the optimization procedure is to be repeated regularly.)

On Figs 24 and 25, at low effective volume concentration, some values of $h_i(\varphi_i)$ (which are the same as $(\eta_R^{(1)})_i$, the relative viscosity of a monomodal suspension in the ith component) are less than unity and log log $\eta_R^{(1)}$ is not real. If we simply ignore the data with $\eta_R^{(1)} < 1$ and include those with $\eta_R^{(1)} > 1$ in the calculation of R, the fitted curve would be biased. It was therefore decided to ignore all data for φ_i less than the value above which no $\eta_R^{(1)}$ data are less than unity. The data so excluded in the optimization procedure are indicated on Figs 24 and 25.

3.5. Results

A summary of the parameters that gave the best fit for each of the three equations is given in Table III, together with the associated minimum R overall.

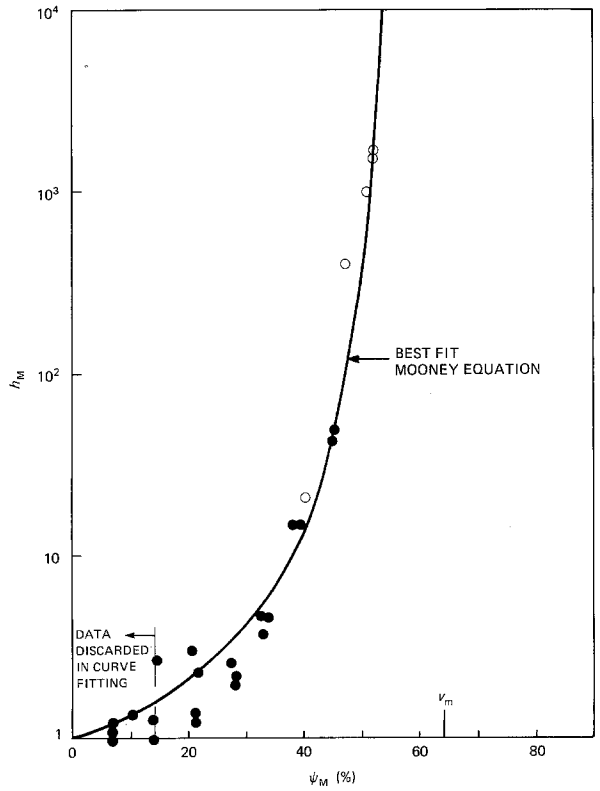

Figure 24 Viscosity function for mediums suspensions (○ experimental, ● derived from bimodal results).

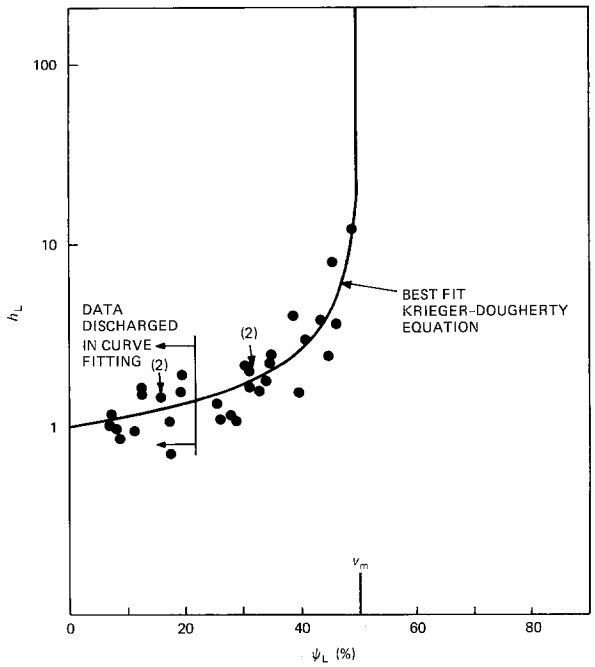

Figure 25 Viscosity function for coarse suspensions (● derived from trimodal results).

It can be seen that the best model equation was different for each size fraction. The fines were best fitted by the Cheng equation, the mediums by Mooney and the coarse by the Krieger–Dougherty equation (Figs 23, 24 and 25). The implications of this finding are discussed in Section 4.3.1.

The Krieger–Dougherty equation was clearly superior for fitting the coarse suspension. This was evident from the distinctly small minimum R compared with the other two and was also apparent when the fitted curves were compared with the data points on the graph (not shown here). The superiority of a given equation was, however, not obvious for the other two suspensions. For the fines, plotting the best-fit curve on Fig. 23 showed that the Krieger–Dougherty equation looked just as good as the Cheng equation. Similarly, the Krieger–Dougherty equation seemed also to fit the mediums, although the Mooney gave the lower minimum R. To check on this the actual residues were plotted on Figs 26 and 27. Fig. 26 shows

TABLE III Results of curve fitting for $h(\psi)$

Equation	Mooney	Krieger–Dougherty	Cheng
parameters	v_m	v_m, k	v_m, A, B
fines	0.559 (0.539)	0.987, 10.8 (0.057)	0.490, 12.8, 38.2 (0.032)
medium	0.638 (0.304)	0.538, 3.6 (0.346)	0.527, 0.0, 0.0 (0.437)
coarse	1.000 (0.777)	0.497, 1.2 (0.425)	1.000, 0.0, 0.0 (0.764)

□ final best-fit equation for each size fraction
( ) minimum average residue

that the residues were indeed less scattered about the Cheng equation. Fig. 27 shows that neither equations were really a good fit because the data points clearly oscillated about the best-fit curves. However, the data points for the Mooney equation were mostly closer to the best-fit curve than the Krieger–Dougherty and so it can be confirmed as the better-fit of the two.

However, looking at Figs 26 and 27, it must be said that the differences between the pairs of equations were marginal. In other words, the Krieger–Dougherty equation could equally well have been accepted as the best fit for the fines and medium suspensions, as it was the best fit for the coarse.

3.6. Prediction of viscosity

The best-fit equations were used to regenerate $\eta_R^{(1)}$ for the monomodal, bimodal and trimodal suspensions for comparison with the experimental data (Figs 26 to 29). The spread about the 1:1 line is of the order of a factor of 2.

The best-fit equations were also used to predict $\eta_R^{(2)}$ against composition curves for the fines + mediums bimodal suspension (Figs 30 to 32) and constant $\eta_R^{(3)}$ contours for the trimodal suspension (Figs 33 to 38). Further discussion of these predictions is given in Section 4.4.

4. Discussion

4.1. Assumptions made in the viscosity measurement

The measurement of the viscosity of high solids content or dense suspensions is not a straightforward problem. In a series of papers [2, 3], it has been shown that the measured viscosity values depend on the geometry of the viscometer and the actual dimensions of the measuring system used. The reason for this is the subject of active research, but it seems clear that this is due to the two-phase nature of suspensions. The particles respond to different flow

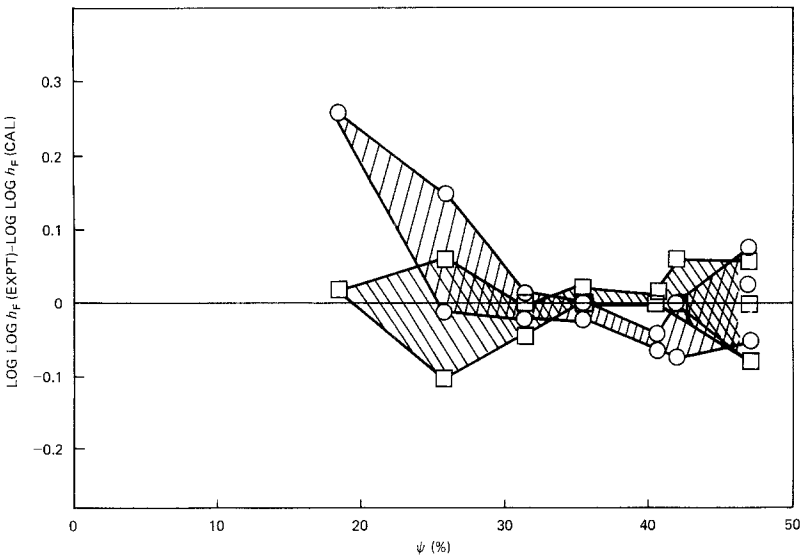

Figure 26 Plot of residues to check goodness of fit to viscosity function for fines suspensions. (○ Krieger-Dougherty equation, □ Cheng equation).

fields by taking up different spatial arrangements or structures. The practical consequence of this is that measurement results obtained in one geometry–size of viscometer cannot be applied to another geometry–size. It is, therefore, very important to bear in mind the end-use of the results in the choice of viscometers. If, for example, the results are to be used for engineering applications such as pipe flow, then a tube viscometer is appropriate. For agitator design and sizing, rotational instruments using scaled-down impellers should be used. For a qualitative assessment of the viscosity, when the general characteristics of a product are being studied, several viscometers of different geometries and sizes should be used in order to obtain a consensus.

In view of this background, the present results cannot, therefore, be considered to be a complete scientific description of the viscosity of the dental suspensions. As they are obtained on a tube viscometer, however, they are relevant to pipe flow situations such as that obtained in a dispensing machine. How relevant they are in relation to the workability as perceived by the dentist is uncertain. Until further research has been carried out, we can use the present results as a qualitative indicator of this charcteristic. It is with these provisos on the significance of these results that the data analysis has been carried out.

In addition to the foregoing, various assumptions, explicit and implicit, were made in this work. They are discussed here.

4.1.1. Solids concentration

It was tacitly asumed in this work that the solids concentration in the viscometer tube was the same as that in the reservoir. Although the delivered concentration can, under appropriate conditions, be the same as that in the reservoir, that in the tube is significantly lower. This was found to be the case for low concentrations, up to about 20% [17]. At very high concentrations, however, it had been shown that even the delivered concentration was different [18]. It was in fact lower, so that as a test progressed the concentration in the reservoir increased, until the solids became so densely packed that jamming resulted [2]. The results of Cloete *et al.* [18] showed that the tube concentration was higher than delivered.

In this work, because of industrial constraints, no check was carried out on the delivered or the tube concentration. As some specific relationship can be expected between the tube concentration and that in

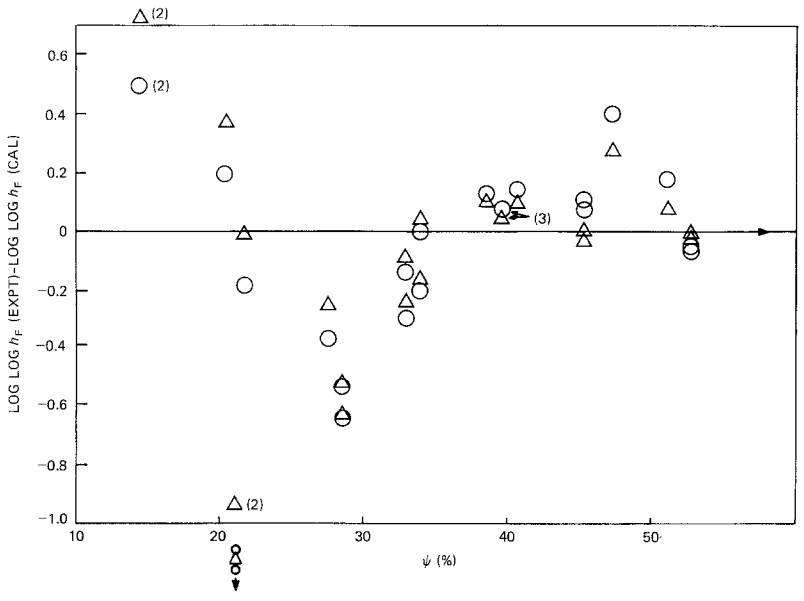

Figure 27 Plot of residues to check goodness of fit to viscosity function for medium suspensions (○ Krieger-Dougherty equation, △ Mooney equation).

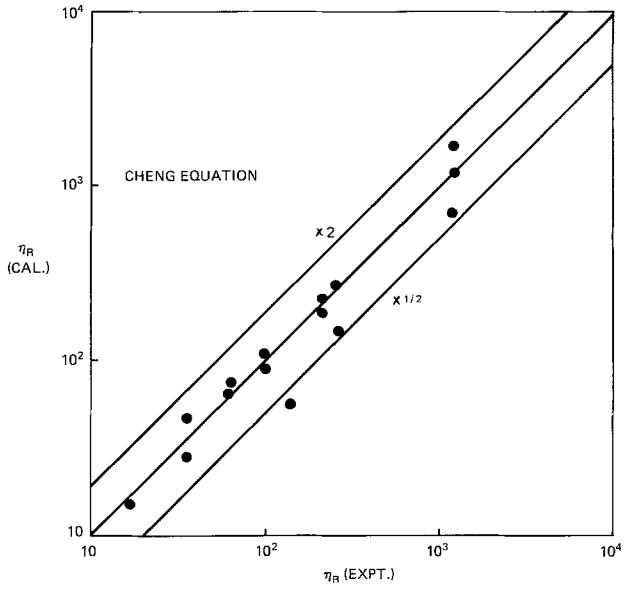

Figure 28 Comparison of experimental data plotted against calculated viscosity for monomodal fine suspensions.

the reservoir given the particular material studied, it was considered that the data analysis based on the reservoir concentration as originally loaded, even if not strictly accurate, can be of practical use.

4.1.2. Pressure measurement

In this work, it was assumed that the pressure measured, which was a radial pressure on the side of the reservoir, can be equated with the axial pressure that is required to calculate the wall shear stress in the tube. While pressure is isotropic in a liquid, this is not the case in a dense suspension. The relation between radial and axial pressure in a densely packed compact of granular solids is given by the Rankin law (given in any soil mechanics book). It can be expected that similar relations exist in dense suspensions. In addition, in viscoelastic fluids, the normal stresses are different in different directions and this is another reason why the radial pressure may not be the same as the axial pressure.

The Davenport Rheometer is not equipped for axial pressure measurement. Again, as some definite relation is expected to exist between axial and radial pressure in the suspensions under study, it was considered that equating the two pressures would give results that are at least useful in a qualitative manner. Future work is being planned to measure the axial as well as the radial pressure.

4.1.3. End-effect correction

An approximation was involved in using the pressure drop in the orifice die as the end-effect correction. This is because the velocity and pressure fields after the orifice are not exactly the same as that in the entrance length of the tube. However, the error involved is thought to be acceptable [6]. In any case the approximation is much less significant compared with the other assumptions discussed above.

4.1.4. Tube diameter effect

Section 2.4.6 shows that there was a definite tube diameter effect on the suspension viscosity and that this cannot be attributed to wall-slip effect alone. In the literature (see refs [9, 10] and those quoted in refs [7, 22–27]) there is considerable discussion of particle migration and it seems clear that this is the cause of the tube diameter effect. On a microrheological level, even the wall slippage phenomenon has and origin in particle movement away from the tube wall, either due to tubular pinch effect [21] or the radial-migration effect [9]. Other authors [2, 7, 22–27] have discussed the topic and showed that a proper understanding of the behaviour of suspensions in tube flow can only be obtained by taking the particle migration effect into account. This has a bearing on solids concentration in the tube also (Section 4.1.1).

As noted in Section 2.4.6, not enough measurements have been carried out in this work to determine the trend of tube diameter effect. The variations observed have been treated as experimental scatter.

4.2. Temperature correction

The assumption made that the relative viscosity was independent of temperature implies that the energy

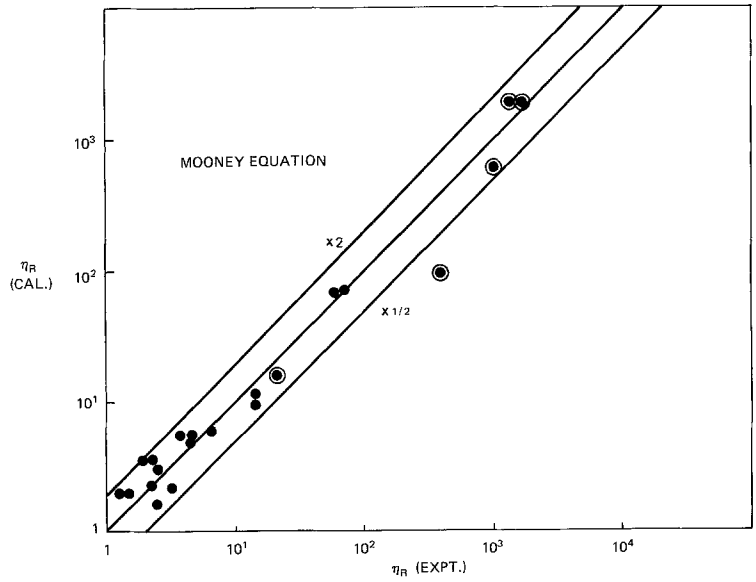

Figure 29 Comparison of experimental data plotted against calculated viscosity for monomodal medium suspensions.

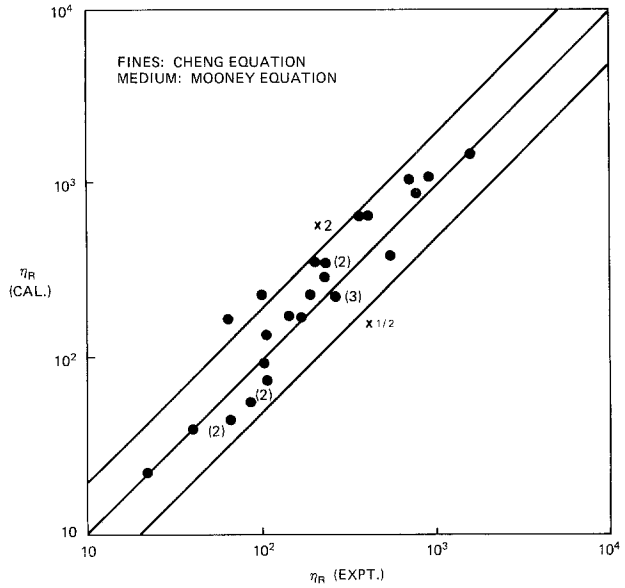

Figure 30 Comparison of experimental data plotted against calculated viscosity for bimodal fine + medium suspensions.

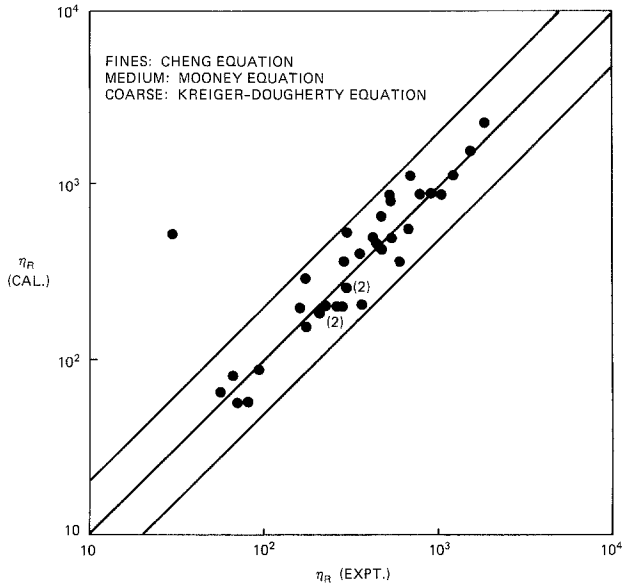

Figure 31 Comparison of experimental data plotted against calculated viscosity for trimodal suspensions.

dissipation in the suspension had an origin in viscous dissipation in the suspending liquid only. It implies that there was no loss when particles collide (i.e. that "dry" frictional effect was absent) and that the adsorbed surfactant molecules do not bring colloidal-chemical effects into play. This assumption is consistent with the assumptions of the Farris theory. How far it is valid can only be assessed experimentally.

4.3. Viscosity–concentration equations, h_i (φ_i)

4.3.1. Significance of the best-fit equations

Three viscosity–concentration equations were assessed in this work and it was found that, on the basis of minimum average residue R, different equations were best fitted to different size fractions (Section 3.5 and Table III). The significance of this is considered in this section.

Many of the viscosity–concentration equations found in the literature were empirically derived and have no more significance other than as being useful for curve fitting, to summarize data for interpolation and limited extrapolation.

Some equations were derived from basic considerations of molecular or particle dynamics and it is generally thought that they have fundamental significance. In a number of cases, parameters of an equation can be evaluated by independent means and compared with values derived from viscosity measurements. This would be a check of the validity of the equation's fundamental significance.

However, in the majority of cases, the derivation of the viscosity–concentration equation did not take *all* the physical and chemical factors into account and the fundamental significance cannot, therefore, be considered to be comprehensive. If one such equation happens to fit a set of experimental data, this can only be considered fortuitous, although of course, the equation is just as useful for data fitting.

In this work, the three equations used were all derived from basic considerations and one might be tempted to discuss their fundamental significance. However, because we do not have independent verification of the values of the parameters and in view of the various reservations discussed in Section 4.1, we did not pursue this line of investigation too far. The three best-fit equations were therefore accepted as empirical and were used in making predictions in Section 4.4.

4.3.2. Effect of Particle size

It would not be easy, even if it is possible, to consider the effect of particle size and/or PSD on $h_i(\varphi_i)$ if equations of different functional forms apply to different fractions. In view of the generally large scatter in the experimental data, however, the Krieger–Dougherty equation could equally well have fitted the suspensions of fines and medium particles (see Section 3.5). The effect of particle size can therefore be assessed in terms of this equation.

The best-fit Krieger–Dougherty parameters for the three size fractions are given in Table III. All the values seem sensible, except for $v_m = 0.987$ for the fines. Such a high value is theoretically possible if a fraction had a very long "tail" towards the very small sizes; then the particles can pack into a very dense packing. It is, however, not possible in practice because when the particles become submicrometre in size, colloidal forces would come into play. Nevertheless, the result suggests that v_m is high for the fines.

In the study of the effect of PSD, the measured size distribution can be reduced to the four moments, corresponding to the mean, standard deviation, skewness and kurtosis. It is known [28] that these quantities are sufficient to represent the distributions. They can be used to correlate with the Krieger–Dougherty parameters.

From the particle size distribution data for the medium and coarse particles, we have extracted d_{50} and (d_{75}/d_{25}) as measures of the mean and standard deviation and tabulated them in Table I. It can be seen that the PSD broadened as the mean size was reduced. No detailed information on particle size distribution was available for the fines, but estimates were made

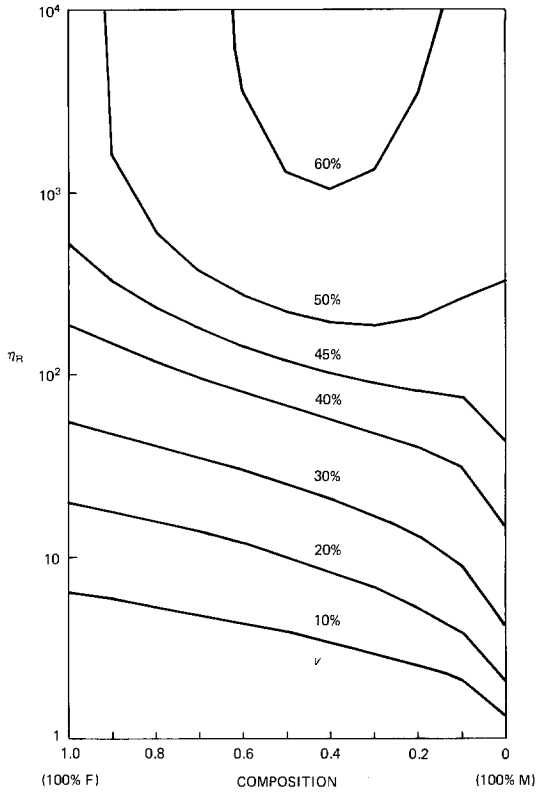

Figure 32 Predicted viscosity for bimodal (fines + mediums) suspensions.

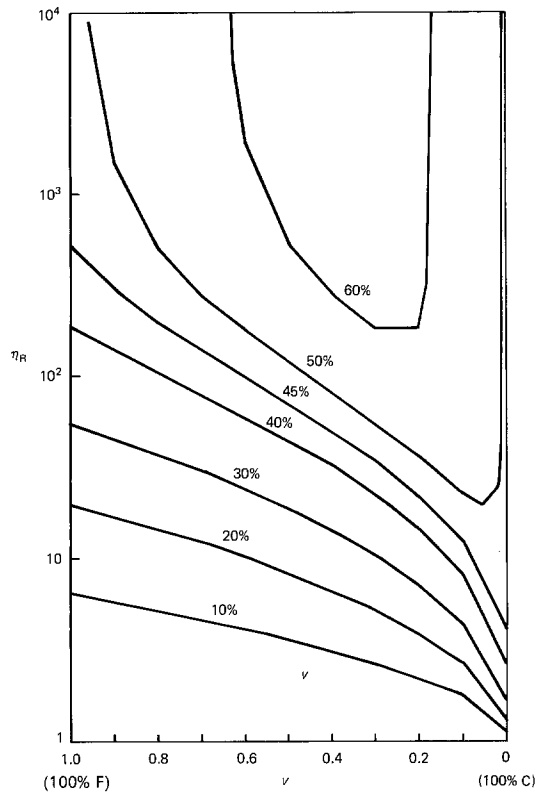

Figure 34 Predicted viscosity for (fines + coarse) suspensions.

using the fact that the limiting ratio of successive sizes should be about 1:10 and that the PSD broadened with decreasing size.

The correlations of V_m and k with PSD are attempted on Fig. 39. V_m is the dense-packing volume fraction and it is expected to correlate with standard deviation or (d_{75}/d_{25}). This seemed to be borne out by the data:

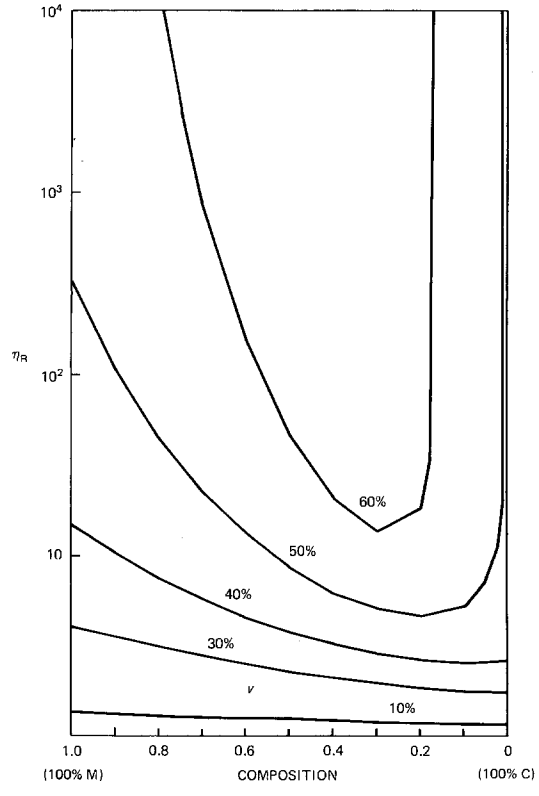

Figure 33 Predicted viscosity for bimodal (mediums + fines) suspensions.

V_m increased as the PSD broadened. k is the intrinsic viscosity and again it is expected to be dependent on standard deviation and not on the mean size. This can be seen from the theory of Farris when applied to mixtures of single-sized fractions of spherical particles [7]. The viscosity concentration curve is shifted such that the intrinsic viscosity is reduced as the number of different size modes in the mixed suspension is increased. The present results in contrast show that k increased as (d_{75}/d_{25}) was increased.

These correlations between V_m and k with PSD can be used to predict the Krieger–Dougherty equation from a knowledge of PSD, and hence to predict mixture viscosity. This justifies further research on the viscosity of suspensions of further different sizes, to confirm the PSD effect.

4.4. Prediction of minimum viscosity

An important aim of the data analysis is to obtain h_i (φ_i) so that bimodal and trimodal compositions that have minimum viscosities can be predicted. The results of the predictions are given in Figs 32 to 38.

The predictions for the bimodal suspensions, Figs 32 to 34, show that at constant low total solids concentration v, the viscosity is in fact lower if the particle fractions are not mixed. On Fig. 32 below $v = 45\%$, the medium particles on their own would give the minimum viscosity at any v; on Fig. 33, this happens with the coarse particles below 30%; and 45% on Fig. 34. The reason for this is that the size fractions were not truly monomodal and the PSD may be near the minimum viscosity for that mixture. Adding further smaller particles to them only moves the viscosity up onto the incline.

The figures show however, that when v is very high, 50% and above, the mixture did possess a viscosity

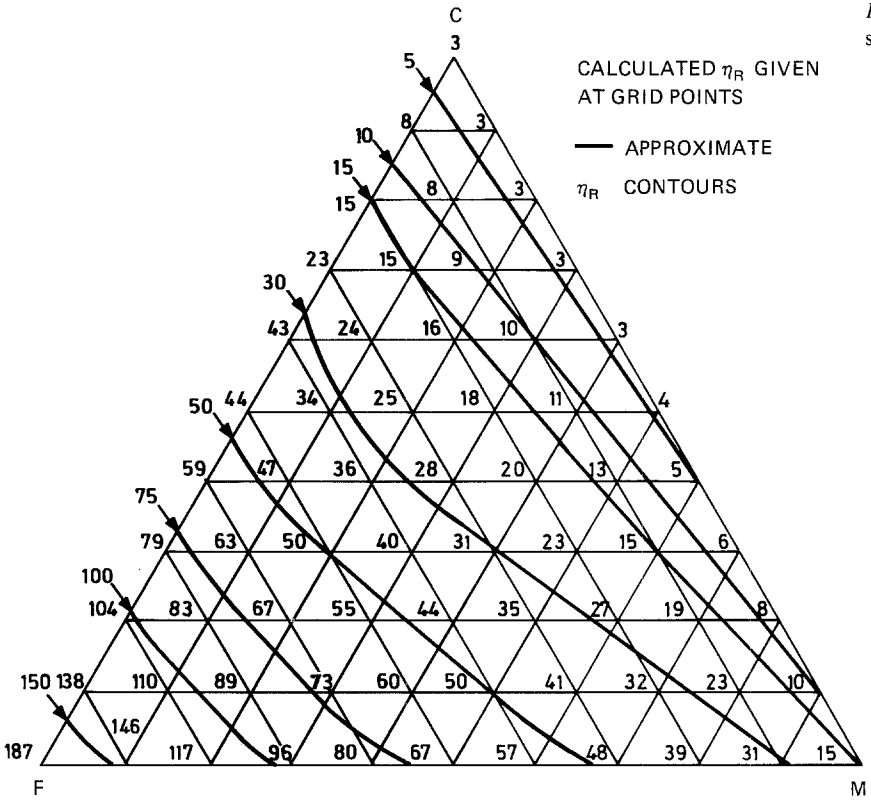

Figure 35 Predicted viscosity for trimodal suspensions at 40% total concentration.

minimum. It is interesting to note, for example that the minimum η_R at 50% is about 200 for the fines + mediums, whereas it is only 5 for the fines + coarse mixtures. This illustrates the wide scope for the design of suspensions.

The predictions for the trimodal mixtures, Figs 35 to 38, show a similar behaviour. At low v, no minimum was found within the triangular diagram and the minimum at a given v is found on the bimodal edge. It is only at high enough v, for example Fig. 38, that the minimum is located within the diagram.

These predictions summarize the measurement results. It is not obvious from the untreated results (Figs 3 to 13, or even Figs 14 to 17) how one can predict the compositions for minimum viscosity. The summary, however, in the form of Figs 32 to 38, will readily allow this to be done.

5. Conclusions

The suspensions studied were found to be highly non-Newtonian. The typical behaviour appeared to be a sigmoid flow curve, with a yield stress at low enough

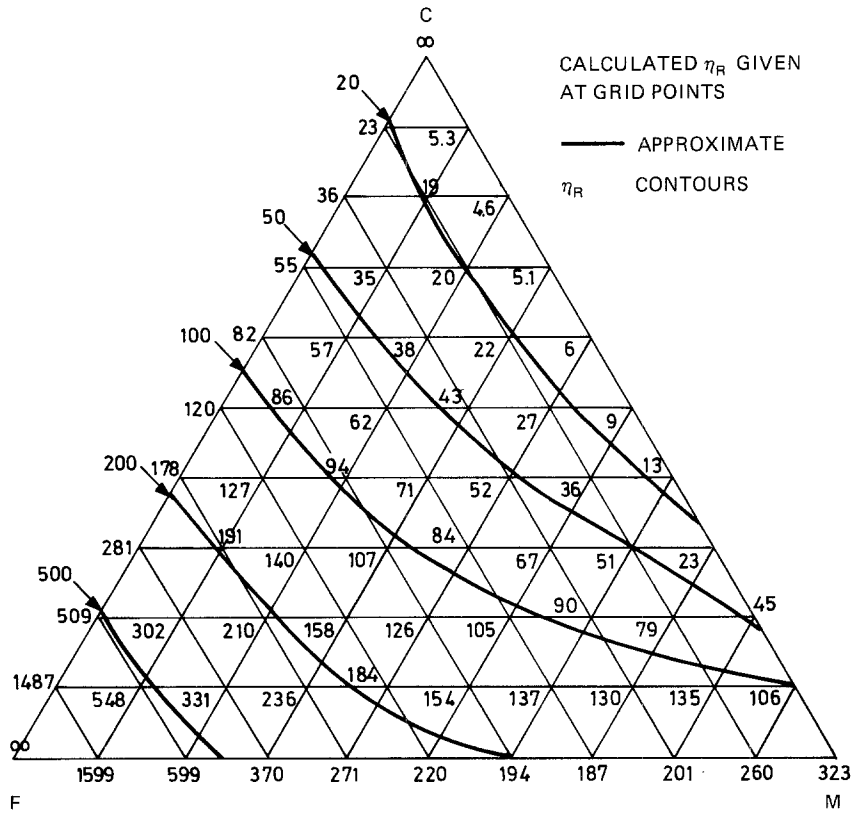

Figure 36 Predicted viscosity for trimodal suspensions at 50% total concentration.

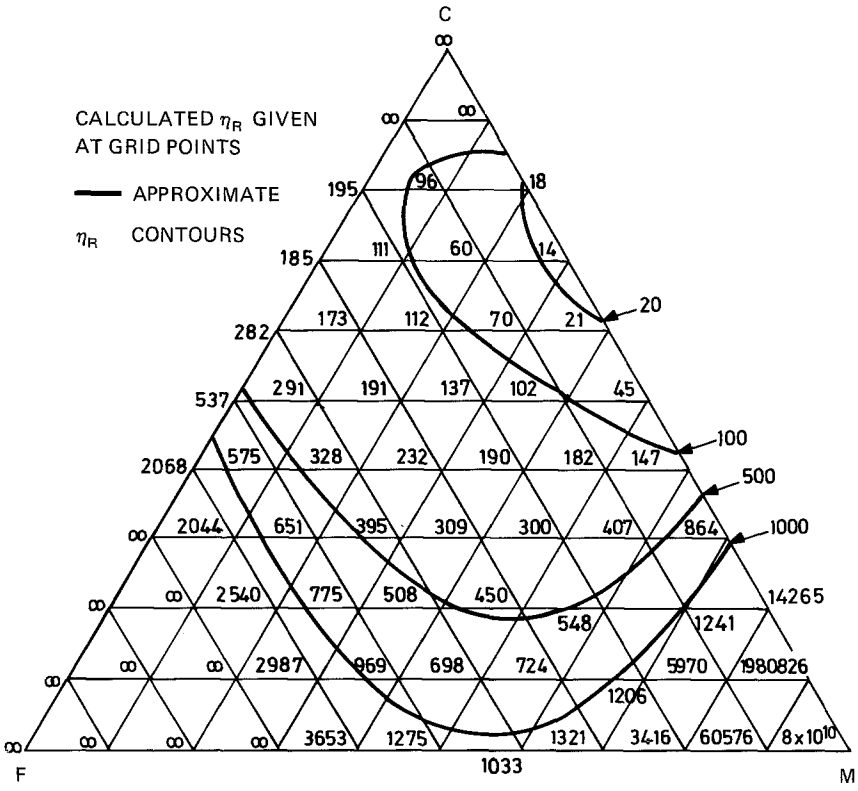

Figure 37 Predicted viscosity for trimodal suspensions at 60% total concentration.

shear rate and curving over to a constant shear stress at high enough shear rate. The inflexion shear rate decreased with increasing concentration.

The viscosity at $100\,sec^{-1}$ (Section 2.4.3) was analysed for particle size and PSD effects. Farris' theory for mixtures of monomodal suspensions was extended to mixtures made up of size fractions that were not uniquely sized involving three different viscosity–concentration functions $h_i(\varphi_i)$, $i = 1, 2, 3$. Those functions were found to be fitted by different equations, Cheng, Mooney and Krieger–Dougherty respectively. They reproduce the experimental data to within a factor of 2 either way, which is good agreement for suspensions of such high solids content.

The best-fit functions, $h_i(\varphi_i)$, were used to calculate the viscosity of bimodal and trimodal suspensions and to predict the compositions at which the viscosity is minimum. The results (Figs 32 to 38) show that at low total solids, the minimum viscosity is not obtained with mixtures in bimodal systems or located within the triangular diagram for trimodal systems. This was due to the size fractions being mixtures in themselves. It was only at very high total solids that viscosity minima were obtained with bimodal mixtures or within the triangular diagram.

It can be concluded that Farris' theory, as extended

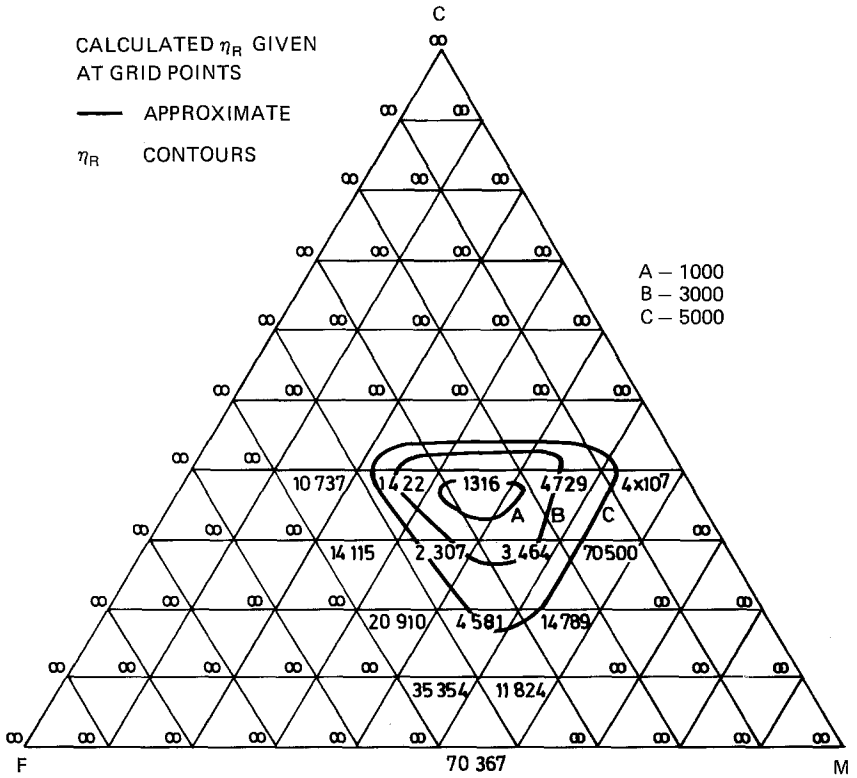

Figure 38 Predicted viscosity for trimodal suspensions at 70% total concentration.

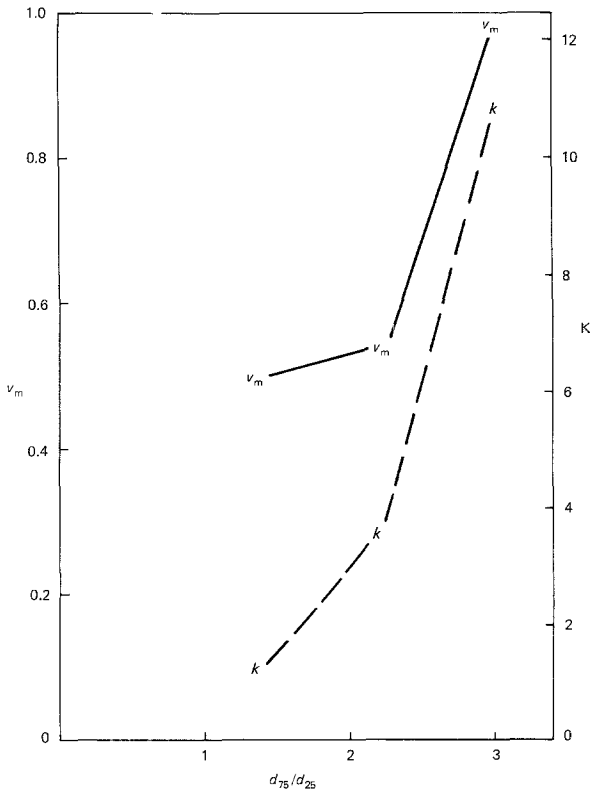

Figure 39 Effect of PSD on Krieger–Dougherty parameters.

in this paper, can be useful in analysing experimental data to determine the viscosity functions $h_i(\varphi_i)$ for different size fractions. They can also be used to determine minimum viscosity conditions when the fractions are combined in different mixtures.

The methodology described for the analysis of suspension viscosity data comprises the reduction of measurement results to the viscosity functions $h_i(\varphi_i)$, for the monomodal size fractions and curve-fitting them to viscosity–concentration equations. The extended Farris theory can be used to predict viscosities for mixtures not measured experimentally, useful in the formulation of industrial products.

References

1. D. C-H. CHENG and R. A. RICHMOND *Rheol. Acta,* **17** (1978) 446–453.
2. D. C-H. CHENG. *Powder. Tech.* **37** (1984) 225–273.
3. *Idem.,* "Flow properties of suspensions of inert spheres". Res. Rept No. LR 548 (MH) Warren Spring Laboratory, Stevenage 1984.
4. J. J. BENBOW, *Lab. Practice,* **12** (1963) 533.
5. D. C-H. CHENG, Proceedings Symposium Physical Properties Liquid and Gases for Plant and Process Design, East Kilbride, 1968. (HMSO, Edinburgh, 1970).
6. F. N. COGSWELL "Polymer Melt Rheology" (George Godwin, London, 1981).
7. R. J. FARRIS, *Trans. Soc. Rheol.,* **12** (1968) 281–301.
8. H. C. BRINKMAN, *J. Chem. Phys.,* **20** (1952) 571.
9. R. ROSCOE, *Brit. J. Appl. Phys.,* **3** (1952) 267–269.
10. D. C-H. CHENG, *Chemistry and Industry* 17 May (1980) 403 -406.
11. M. MOONEY, *J. Coll. Sci.,* **6** (1951) 162–170.
12. I. M. KRIEGER and T. J. DOUGHERTY, *Trans. Soc. Rheol.* **3** (1959) 137–152.
13. D. C-H. CHENG, *Bull. Br. Soc. Rheol.,* **27** (1984) 1–8.
14. D. G., THOMAS, *J. Coll. Sci.,* **20** (1965) 267–277.
15. C. HENDRIX, *Chem. Tech.* August (1980) 488–497.
16. G. S. G. BEVERAGE and R. S. SCHECHTER, "Optimisation: Theory and Practice" (McGraw-Hill, New York, 1970).
17. V. SESHADRII and S. P. SUTERA, *Trans. Soc. Rheol.,* **14** (1970) 351–371.
18. F. L. D. CLOETE, A. I. MILLER and M. STREAT, *Trans. Instn. Chem. Engrs.,* **45** (1967) T392–400.
19. G. SEGRE and A. SILBERBERG, *J. Fluid Mech.,* **14** (1962) 115–135.
20. F. GAUTHIER, H. L. GOLDSMITH and S. G. MASON, *Trans. Soc. Rheol.,* **15** (1971) 297–330.
21. R. L. WHITMORE, in "Rheology of Disperse Systems," edited by C. C. Mill (Pergamon, London 1959) pp. 49–60.
22. H. W. THOMAS, *Biorheol.,* **1** (1962) 41–56.
23. G. SEGRE and A. SILBERBERG, *J. Colloid Sci.,* **18** (1963) 312–317.
24. S. IWANAMI and M. TACHIBANA, *Bull. JSME,* **12** (1969) 224–239.
25. R. PATZOLD, *Rheol. Acta,* **19** (1980) 322–344.
26. H. GOTO and H. KUNO, *J. Soc. Rheol. Jap.,* **11** (1983) 45–50.
27. *Idem., J. Rheol.,* **28** (1984) 197–205.
28. M. G. KENDALL and A. STUART, "The Advanced Theory of Statistics, Vol. 1 Distribution Theory," (Griffin and Co, London, 1963) p. 56.

Received 30 June 1988
and accepted 14 April 1989